

# **NAVAL POSTGRADUATE SCHOOL**

## **Monterey, California**



## **THESIS**

**AN INVARIANT DISPLAY STRATEGY FOR  
HYPERSPECTRAL IMAGERY**

by

Athanasis E. Konsolakis

September 2001

Thesis Advisor:

Roberto Cristi

Second Reader:

J. Scott Tyo

**Approved for public release; distribution is unlimited**

## Report Documentation Page

<b>Report Date</b> 30 Sep 2001	<b>Report Type</b> N/A	<b>Dates Covered (from... to)</b> - -
<b>Title and Subtitle</b> An Invariant Display Strategy for Hyperspectral Imagery		<b>Contract Number</b>
		<b>Grant Number</b>
		<b>Program Element Number</b>
<b>Author(s)</b> Athanasios E. Konsolakis		<b>Project Number</b>
		<b>Task Number</b>
		<b>Work Unit Number</b>
<b>Performing Organization Name(s) and Address(es)</b> Research Office Naval Postgraduate School Monterey, Ca 93943-5138		<b>Performing Organization Report Number</b>
		<b>Sponsor/Monitor's Acronym(s)</b>
<b>Sponsoring/Monitoring Agency Name(s) and Address(es)</b>		<b>Sponsor/Monitor's Report Number(s)</b>
<b>Distribution/Availability Statement</b> Approved for public release, distribution unlimited		
<b>Supplementary Notes</b>		
<b>Abstract</b>		
<b>Subject Terms</b>		
<b>Report Classification</b> unclassified	<b>Classification of this page</b> unclassified	
<b>Classification of Abstract</b> unclassified	<b>Limitation of Abstract</b> UU	
<b>Number of Pages</b> 90		

**REPORT DOCUMENTATION PAGE**
*Form Approved OMB No. 0704-0188*

Public reporting burden for this collection of information is estimated to average 1 hour per response, including the time for reviewing instruction, searching existing data sources, gathering and maintaining the data needed, and completing and reviewing the collection of information. Send comments regarding this burden estimate or any other aspect of this collection of information, including suggestions for reducing this burden, to Washington headquarters Services, Directorate for Information Operations and Reports, 1215 Jefferson Davis Highway, Suite 1204, Arlington, VA 22202-4302, and to the Office of Management and Budget, Paperwork Reduction Project (0704-0188) Washington DC 20503.

<b>1. AGENCY USE ONLY (Leave blank)</b>	<b>2. REPORT DATE</b> September 2001	<b>3. REPORT TYPE AND DATES COVERED</b> Master's Thesis
<b>4. TITLE AND SUBTITLE:</b> An Invariant Display Strategy for Hyperspectral Imagery		<b>5. FUNDING NUMBERS</b>
<b>6. AUTHOR(S)</b> Athanasios E. Konsolakis		
<b>7. PERFORMING ORGANIZATION NAME(S) AND ADDRESS(ES)</b> Naval Postgraduate School Monterey, CA 93943-5000		<b>8. PERFORMING ORGANIZATION REPORT NUMBER</b>
<b>9. SPONSORING / MONITORING AGENCY NAME(S) AND ADDRESS(ES)</b> N/A		<b>10. SPONSORING / MONITORING AGENCY REPORT NUMBER</b>
<b>11. SUPPLEMENTARY NOTES</b> The views expressed in this thesis are those of the author and do not reflect the official policy or position of the Department of Defense or the U.S. Government.		
<b>12a. DISTRIBUTION / AVAILABILITY STATEMENT</b> Approved for public release; distribution is unlimited		<b>12b. DISTRIBUTION CODE</b>

**13. ABSTRACT (maximum 200 words)**

Remotely sensed data produced by hyperspectral imagers contains hundreds of contiguous narrow spectral bands at each spatial pixel. The substantial dimensionality and unique character of hyperspectral imagery requires display techniques that differ from those provided by traditional image analysis tools. This study investigated techniques enabling the display of hyperspectral images without the interference of in-scene characteristics that lead to biased representations depending on the content of every image under analysis. Utilizing the Principal Components Analysis transformation it is possible to simplify the representation requirements while maintaining the information contained in the scene. The introduction of an external eigenvector, containing few spectral characteristics, into the original scene data removes most of the spectral bias allowing for an accurate detection of the constituent elements. The subsequent shift of the resulting data to match the respective hue directions in the dataspace allows for image color fidelity based on the true composition of the image while all the environmental influence has been removed and the final outcome is readily perceived by the human vision.

<b>14. SUBJECT TERMS</b> Hyperspectral Imagery, Hyperspectral Imagers, Eigenvectors		<b>15. NUMBER OF PAGES</b> 89
		<b>16. PRICE CODE</b>
<b>17. SECURITY CLASSIFICATION OF REPORT</b> Unclassified	<b>18. SECURITY CLASSIFICATION OF THIS PAGE</b> Unclassified	<b>19. SECURITY CLASSIFICATION OF ABSTRACT</b> Unclassified
		<b>20. LIMITATION OF ABSTRACT</b> UL

THIS PAGE INTENTIONALLY LEFT BLANK

**Approved for public release; distribution is unlimited**

**AN INVARIANT DISPLAY STRATEGY FOR HYPERSPECTRAL IMAGERY**

Athanasis E. Konsolakis  
Lieutenant, Hellenic Navy  
B.S., Naval Engineering, Hellenic Naval Academy, 1991

Submitted in partial fulfillment of the  
requirements for the degree of

**MASTER OF SCIENCE IN ELECTRICAL ENGINEERING**

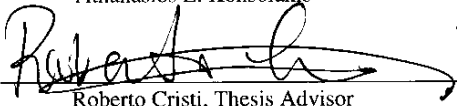
from the

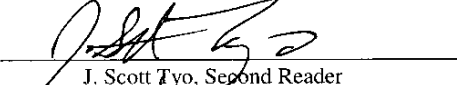
**NAVAL POSTGRADUATE SCHOOL**  
**September 2001**

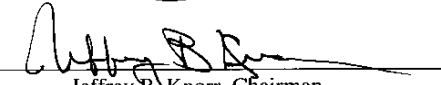
Author:

  
Athanasis E. Konsolakis

Approved by:

  
Roberto Cristi, Thesis Advisor

  
J. Scott Tyo, Second Reader

  
Jeffrey R. Knorr, Chairman

Department of Electrical and Computer Engineering

THIS PAGE INTENTIONALLY LEFT BLANK

## **ABSTRACT**

Remotely sensed data produced by hyperspectral imagers contains hundreds of contiguous narrow spectral bands at each spatial pixel. The substantial dimensionality and unique character of hyperspectral imagery requires display techniques that differ from those provided by traditional image analysis tools. This study investigated techniques enabling the display of hyperspectral images without the interference of in-scene characteristics that lead to biased representations depending on the content of every image under analysis. Utilizing the Principal Components Analysis transformation it is possible to simplify the representation requirements while maintaining the information contained in the scene. The introduction of an external eigenvector, containing few spectral characteristics, into the original scene data removes most of the spectral bias allowing for an accurate detection of the constituent elements. The subsequent shift of the resulting data to match the respective hue directions in the dataspace allows for image color fidelity based on the true composition of the image while all the environmental influence has been removed and the final outcome is readily perceived by the human vision.

**THIS PAGE INTENTIONALLY LEFT BLANK**

## TABLE OF CONTENTS

I.	INTRODUCTION .....	1
II.	BACKGROUND .....	3
A.	PROBLEM STATEMENT .....	3
B.	HYPERSPECTRAL IMAGERY OVERVIEW.....	3
C.	DEFINITIONS .....	5
1.	Spectral Imagery .....	6
2.	Statistical Interpretation.....	9
3.	Related Signal Processing and Linear Algebra Concepts .....	17
a.	<i>Linear Transformations of Random Variables</i> .....	17
b.	<i>Eigenvectors and Eigenvalues</i> .....	18
c.	<i>Unitary Transformations</i> .....	19
d.	<i>A Geometric Interpretation of the Unitary Transform</i> .....	19
4.	Principal Components Analysis.....	21
a.	<i>General</i> .....	21
b.	<i>Background</i> .....	22
c.	<i>Operation</i> .....	26
5.	Color Vision.....	32
a.	<i>Description</i> .....	32
b.	<i>Comparison to Principal Components</i> .....	36
III.	MAPPING STRATEGY .....	39
A.	PSEUDOCOLOR AND OPPONENT COLOR MAPPING STRATEGIES .....	39
B.	ORIGINAL PRINCIPAL COMPONENTS STRATEGY.....	42
C.	MODIFICATION USING EXTERNAL FIRST PC .....	43
1.	Scene Selection .....	44
2.	External Eigenvector Selection.....	48
3.	Gramm-Schmidt Transform.....	49
4.	Scatter Plots .....	50
5.	n-Dimensional Visualizer and Endmembers Selection .....	51
6.	Cone Vertex Coordinates Determination.....	54
7.	Data Shifting .....	57
8.	HSV System Determination .....	58
9.	HSV to RGB Transformation.....	58
10.	RGB Visualization.....	59
IV.	LIMITATIONS AND FUTURE WORK.....	63
V.	SUMMARY AND CONCLUSIONS .....	67
LIST OF REFERENCES .....		69
INITIAL DISTRIBUTION LIST.....		73

THIS PAGE INTENTIONALLY LEFT BLANK

## LIST OF FIGURES

Figure 2.1.	Major Imagery Analysis Paradigms .....	4
Figure 2.2.	A Typical 6-Band Multispectral Image Produced by Landsat TM. ....	7
Figure 2.3.	Lake Tahoe Representations (left to right): Grayscale (Band 37), RGB (Bands 176, 91, 31), RGB (Bands 25, 120, 200). ....	8
Figure 2.4.	The Concept of a Pixel Vector. From Vane and Goetz, 1988. ....	9
Figure 2.5.	Scatter Plots of Canon City Landsat TM Data Showing Highly Correlated (2 <sup>nd</sup> & 3 <sup>rd</sup> ) and Less Correlated (1 <sup>st</sup> & 4 <sup>th</sup> ) Band Combinations. ....	15
Figure 2.6.	Typical Pixel Vectors From Hyperspectral Images. ....	16
Figure 2.7.	Linear Transformation of a Two-dimensional Vector. ....	17
Figure 2.8.	The Unitary Transformation as a Rotation of Axes. From Richards, 1993....	20
Figure 2.9.	PC Transformation Depicted as a Linear Transformation. ....	21
Figure 2.10.	The Karhunen-Loeve Expansion in Terms of Discrete Signals. After Therrien, 1992.....	24
Figure 2.11.	First 20 PC Images of Lake Tahoe. ....	27
Figure 2.12.	Lake Tahoe False Color Image. ....	29
Figure 2.13.	Original Lake Tahoe Image in Visible Spectrum. ....	30
Figure 2.14.	Cross Section of the Human Eye. ....	33
Figure 2.15.	Sensitivity of Rods and Cones (Pratt, 1991).....	34
Figure 2.16.	Spectral Absorption Curves (Scott, 1997). ....	35
Figure 2.17.	Human Visual Spectrum (Scott, 1997). ....	35
Figure 2.18.	Conical Colorspace. ....	37
Figure 3.1.	Pseudocolor Representation of Davis-Monthan Scene Obtained by Mapping the First Three PCs into (R, G, B). ....	39
Figure 3.2.	Pseudocolor Representation of Davis-Monthan Scene Obtained with Equation 3.1.....	40
Figure 3.3.	RGB Image with Original Data Bands 150, 38 and 10. ....	41
Figure 3.4.	HSV Image Transformed with Scene RGB Data. ....	42
Figure 3.5.	Lake Tahoe Scene. ....	44
Figure 3.6.	1st, 2nd, and 3rd Eigenvectors from Tahoe Scene. ....	45
Figure 3.7.	1st Eigenvector from Davis-Monthan AFB Scene. ....	46
Figure 3.8.	Davis-Monthan AFB Scene. ....	47
Figure 3.9.	1st, 2nd, and 3rd Eigenvectors from Davis-Monthan AFB Scene. ....	48
Figure 3.10.	Resulting Eigenvectors from Gramm-Schmidt Transformation. ....	50
Figure 3.11.	Scatterplots of the Resulting Eigenvectors. ....	51
Figure 3.12.	Endmembers as Highlighted by n-D Visualizer. ....	53
Figure 3.13.	ROIs Highlighted by the n-D Visualizer. ....	54
Figure 3.14.	Trimmed-down Data Cloud Indicating MSE Approximations. ....	56
Figure 3.15.	Selected Directions Approximating Cone Vertex in 3-Dimensions. ....	57
Figure 3.16.	R, G, B Images.....	60
Figure 3.17.	Processed and Rotated Color Image. ....	61
Figure 4.1.	Images Comparison: Top-Original Image, Bottom-Processed Image.....	65

THIS PAGE INTENTIONALLY LEFT BLANK

## LIST OF TABLES

Table 2.1.	Covariance and Correlation Matrices of Landsat TM Data.....	13
Table 3.1.	HSV to RGB Transformation. ....	59

THIS PAGE INTENTIONALLY LEFT BLANK

## **ACKNOWLEDGMENTS**

The author would like to thank Associate Professor of Physics Richard C. Olsen of the Naval Postgraduate School for his time and insight into hyperspectral imagery analysis. Special thanks also to Scott Tyo for his dedication towards the completion of this work beyond the difficulties that emerged in the latter part of our cooperation.

THIS PAGE INTENTIONALLY LEFT BLANK

## EXECUTIVE SUMMARY

An invariant methodology has been developed in response to the need for coherent and consistent display of the hundreds of contiguous narrow spectral bands present within hyperspectral imagery. This methodology builds upon existing hyperspectral imagery processing techniques and introduces a more robust first look capability for unsupervised classification.

This study investigated techniques enabling the display of hyperspectral images without the interference of in-scene characteristics that lead to biased representations depending on the content of every image under analysis. The execution of this work was accomplished by utilizing ENVI software and the related IDL programming language.

A selection of particular scenes was done based on their content in a way that would provide generalized results for later application of the technique to a broad suite of images. The scene processed in this study depicts an area in Lake Tahoe where water and vegetation are the predominant elements. These particular elements result in strong fluctuations on the eigenvectors generated by the Principal Components Analysis (PCA) described in the study. With such variability in the collected imagery it becomes difficult to develop a strategy capable of performing unsupervised analysis and detection of certain features and materials on the surface.

The introduction of an eigenvector irrelevant to the particular scene and produced externally through the PCA transformation of a different scene provided the means to remove much of the variability of the original image and suppress it to elements that have negligible influence on the final outcome. The external eigenvector was derived from a Davis-Monthan AFB scene that contained mainly pixels depicting desert sand. Consequently the spectral profile of this scene contained almost intact the solar radiance mostly unaffected by ground element- or atmosphere-induced absorption. This external eigenvector was “forced” into the Lake Tahoe scene data through a Gramm-Schmidt transformation resulting in a new Principal Component orthogonal set comprised of the new 1<sup>st</sup>, 2<sup>nd</sup>, and 210<sup>th</sup> eigenvectors. Utilizing this set of eigenvectors, a 3-dimensional

colorspace was generated where the 210<sup>th</sup> eigenvector comprised the brightness value direction mostly unaffected by any particularities of the processed image.

The shifting of the cone-shaped colorspace performed in this study in a way that its vertex coincides with the origin of the dataspace, allowed an accurate determination of the various image components hue differences since these components corresponded to distinct pixel groups radiating outwards from the colorspace vertex as evidenced in the scatterplots generated by ENVI.

The resulting processed image displayed a certain amount of color consistency enabling the analyst to recognize particular patterns and elements without any prior knowledge of the scene content. The presented technique demonstrates the usefulness of the strategy pursued while the development of a completely automated unsupervised technique may become possible in the near future as soon as some of the steps followed in this study can be accomplished by software only instead of the analyst's intervention.

## I. INTRODUCTION

Hyperspectral data, a particular type of spectral imagery, is produced when solar electromagnetic energy reflected from the earth's surface is dispersed into many contiguous narrow spectral bands by an airborne spectrometer (Vane and Goetz, 1988, p. 3).

Each picture element (pixel) of a hyperspectral image can be thought of as a high resolution trace of radiation versus wavelength, or a spectrum (Rinker, 1990, p. 6).

The characteristic wavelength dependent changes in the emissivity and reflectivity of a given material can be related to the chemical composition and types of atomic and molecular bonds present in that material (Gorman, et. al., 1995, p. 2805).

The basic goal of this study is to develop an invariant display strategy for presenting a wide variety of high-dimensional images in a way consistent to the human eye perception, highlighting important scene properties. This study follows an incremental approach in presenting the constituents of hyperspectral imagery and the methodology followed in developing an invariant display strategy. Chapter II provides the background of this study by stating the problem of invariant display strategy, by providing an overview of hyperspectral imagery in general and by outlining important concepts such as the fundamentals of human vision, Principal Components Analysis and the statistical background of spectral imagery. Chapter III details the mapping strategy followed in this study providing simultaneously the outline of the already existing Principal Components strategy, which forms the basis for further variations. Chapter IV discusses the results of the display strategy after its application to a variety of hyperspectral scenes. Chapter V concludes the study providing with the connections and possible directions to display strategies that will lead to more invariant and universal methods for representing hyperspectral scenes.

THIS PAGE INTENTIONALLY LEFT BLANK

## II. BACKGROUND

### A. PROBLEM STATEMENT

During the past century, several strategies were developed to analyze the information carried by the number of spectral samples contained at each pixel in a particular scene. Such strategies have been used for target identification, material classification, terrain mapping, etc. Once a classification algorithm or image processing tool has been applied to a spectral image, the resulting processed data is invariably mapped into a pseudocolor image. While many display methodologies are quite powerful, as of today there is no standard tool devised to present spectral imagery in false-color representations.

Currently, the use of false color displays is generally reserved as a tool for presenting data after processing. A specifically tailored colormap is created to emphasize the performance of the classification system, after a particular algorithm has classified a scene. Displaying the data is commonly used as an initial processing step, in an attempt to distinguish scene elements. However, visualization by itself is rarely used as a tool that could allow a spectral analyst to perform identification before implementing more powerful processing strategies. Most colormaps in use today have been developed based on the mathematics of spectral images without considering the workings of the human vision system. It has been demonstrated that failure to consider how the observer processes data visually can make information difficult to find in an image, even when the data are clearly available (Tyo, et. al., 1998).

### B. HYPERSPECTRAL IMAGERY OVERVIEW

A review of the historical perspective and the various stages in the analysis of hyperspectral images follows so that the need of an invariant false-color mapping strategy is acknowledged. Figure 2.1 illustrates the major image analysis paradigms over the past seventy years (Stefanou, 1997, p. 13). This is a brief overview of the major ideas behind hyperspectral imagery analysis, not including the whole history of it, however. It is interesting to point out that there is no visual representation strategy within any of the paradigms.

Photointerpretation (1930s)

- : 2-D Images
- : good qualitative analysis (human)
- : poor quantitative analysis

Digital Imagery (1960s)

- : 2-D Images
- : Pattern Recognition, Computer Vision
- : Emphasis on Classification Techniques

Multispectral Imagery (1970s)

- : 3-D Images
- : Principal Components Analysis
- : Land Usage Classification

Hyperspectral imagery (1980s)

- : 3-D
- : Need to reduce data dimensionality
- : Software Packages with Spectral Libraries
- : Need efficient processing techniques

Figure 2.1. Major Imagery Analysis Paradigms.

Photointerpretation constituted the beginning of imagery analysis in the early part of the past century. A human operator was necessary to extract information of interest while analyzing aerial photography. The strength of the human element in interpretation was the ability to recognize large-scale patterns (Richards, 1993, p. 75) and make inferences based on these patterns. The inherent inability to accurately quantify the results in a consistent manner however is the weakness of human image interpretation.

The computing power that began to become available in the 1960's and the ability to represent data in a digital fashion provided impetus for automation of the photointerpretation task into digital imagery analysis. Here, the computer was programmed to work within narrow parameters, such as counting the number of occurrences of certain brightness values, a task where it outperformed any human analyst without any deterioration in accuracy. The fields of pattern recognition and computer vision became important, while a statistical description of the data was needed to form the basis of classification schemes that could accurately determine the number of pixels

in the scene belonging to a certain class. Linear prediction and principal components analysis (PCA) were tools that assisted in the automated detection of a target in the two-dimensional digital images.

The introduction of multispectral imagery with Landsat-obtained data in the 1970's added a spectral dimension to the problem of imagery analysis. That meant that if the number of spectral samples at each pixel was  $N$ , the multispectral images posed  $N$  times the amount of data for analysis. A significant role in reducing the dimensionality of the data was played by PCA by decreasing from  $N$  number of samples to  $M < N$  linear combinations. This was achieved by exploiting redundancy within the data and assisted in the classification of large land areas. The relationship between PCA techniques and classification techniques was a sequential operation in that PCA was first applied to an image to remove the redundant information or create a better class separation before application of a classifier. This preprocessing application of PCA still continues today.

The 1980's and hyperspectral imagery presented a new challenge to the existing methods of analyzing data. Hyperspectral imagery increased the number of spectral bands from less than 10 to more than 200, increasing the volume of data by a factor of 20-50. Therefore, the need for data compression emerged and became an important concern. The search for new techniques to deal with the large amount of information and the corresponding amount of redundancy dictated new views of the analysis paradigm. Ideas from the signal processing community provided a means of handling the large amount of data and confronting the mixed pixel problem. Software packages dedicated to the analysis of hyperspectral imagery incorporated spectral libraries and found particular interest in the geological remote sensing community. One of these packages is ENVI, which is primarily used in this study providing with powerful image processing tools in an IDL language environment.

## C. DEFINITIONS

Understanding the fundamental ideas behind the various spectral imagery analysis techniques is important because all imagery analysis and image display methodologies are based on it. The fundamental ideas borrow concepts from statistics, linear algebra, and signal processing theory. Presenting these ideas in the context of spectral imagery allows the detailed discussion of display strategies that follow.

In this section multispectral and hyperspectral images are presented as a means for further elaborating on certain properties of the spectral concept. The images are also studied from a statistics standpoint that further assists in better understanding the image content and the statistical principles used in spectral imagery analysis. Some linear algebra and signal processing concepts are defined to provide a framework through which certain spectral imagery analysis techniques and display methodologies are presented. These guidelines offer a means of defining key concepts that appear throughout this study. Due to the nature of this study there is an extensive use of illustrated examples that also helps making the above mentioned definitions simple and comprehensive.

## **1. Spectral Imagery**

The acquisition of images at multiple wavelengths by spectrometers onboard aircraft or spacecraft is defined as spectral imagery. Two major classes of such measurements can be distinguished: the traditional multispectral images, such as those acquired by the Thematic Mapper (TM) radiometer on the Landsat satellites, and the hyperspectral imagery, produced by imaging spectrometers such as in the Airborne Visible/Infrared Imaging Spectrometer (AVIRIS) and the Hyperspectral Digital Imaging Collection Experiment (HYDICE) systems. Typical Landsat TM and HYDICE images will be used in this section to introduce some of the concepts needed for this study. Hyperspectral data sets from HYDICE only will be used to illustrate display strategies in later sections. The Landsat TM scene in Figure 2.2 is a six-band, 640-pixel 400-pixel image of Canon City, Colorado that is provided with ENVI software on the ENVI-DATA CD-ROM. The scene is an image of a city surrounded by mountains. The six distinct image planes present in Figure 2.2 represent the various wavelength ranges sensed by Landsat TM. Notice how objects that appear bright in one band may appear dark in another band. The mountain ridgeline, found on the left side of the image, illustrate this effect. Through this sort of contrasting, Landsat imagery offers a very basic means of discerning the spectral character of a particular class of material.

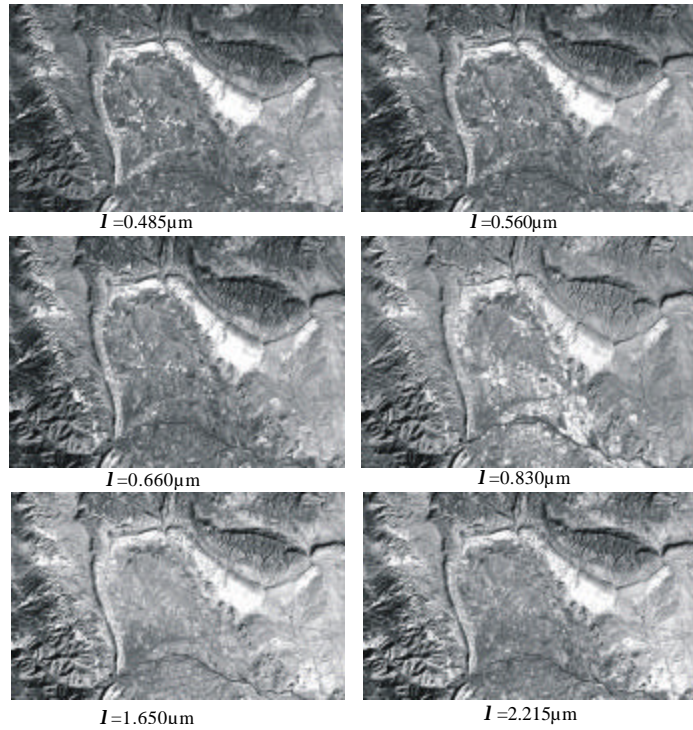


Figure 2.2. A Typical 6-Band Multispectral Image Produced by Landsat TM.  
(Note different shadings between bands.)

A representative HYDICE scene of Lake Tahoe was chosen for comparison. The scene shows a part of the lake itself bordering to a portion of the forest with a shoreline between them. Figure 2.3 shows three representations of the hyperspectral image consisting of 210 bands, 320 lines, and 320 samples each. The first image is a grayscale representation of band 37, the second image is a red, green, blue composite formed using bands 176, 91, and 31, and the third image is a red, green, blue composite formed using bands 25, 120, and 200. The Lake Tahoe representation in Figure 2.3 shows only a small subset of the wide range of color mappings available to an analyst.

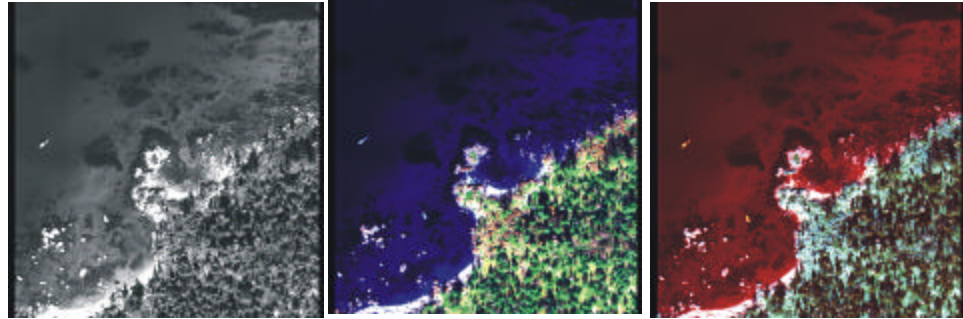


Figure 2.3. Lake Tahoe Representations (left to right): Grayscale (Band 37), RGB (Bands 176, 91, 31), RGB (Bands 25, 120, 200).

One way of visualizing data that has two spatial and one spectral dimension is as a cube. Due to ‘finer’ resolution of spectral frequencies, the ability to identify materials based on spectral detail is more effective with hyperspectral imagery as opposed to multispectral imagery (Goetz, 1995). Figure 2.4 emphasizes the high spectral resolution of hyperspectral data by extracting information in the spectral dimension, or downward in the axes of the cube. It shows the construction of an observed spectrum associated with a particular spatial location, called a pixel vector.

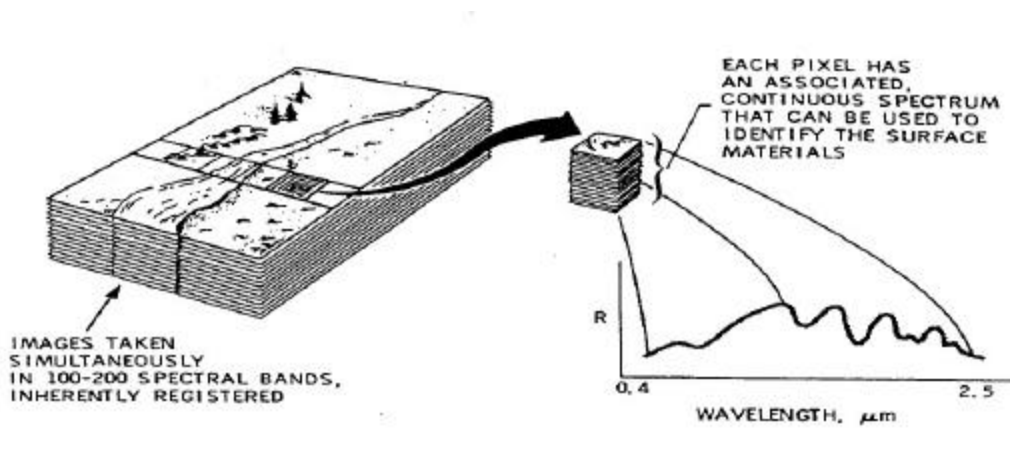


Figure 2.4. The Concept of a Pixel Vector. From Vane and Goetz, 1988.

## 2. Statistical Interpretation

In order to assist in the quantitative discussion of characterizing the data statistically, we need to formally define the concept of the observed pixel vector. Assume that the observed pixel vector  $\mathbf{x}$  is a real valued random vector

$$\mathbf{x} = \begin{bmatrix} \mathbf{x}_1 \\ \vdots \\ \mathbf{x}_L \end{bmatrix} \quad (2.1)$$

where the components  $\{\mathbf{x}_1, \dots, \mathbf{x}_L\}$  correspond to measured brightness values in each of  $L$  spectral bands. Since a stochastic view of the data assumes that these vectors are random entities, they can be characterized by describing their behavior using statistical concepts. Exact statistical descriptions of their behavior are unavailable in real applications, so we must rely on methods that estimate the statistics of the observed random vectors.

There are three major statistical definitions of interest in this respect. The first is the concept of expectation. The expectation of a random vector is called the mean or the average value that the random vector assumes and is denoted as  $E\{\mathbf{x}\}$ . The mean is also called the first moment since it involves only the random vector itself and not products of the components of the vector  $\mathbf{x}$  (Therrien, 1992, p. 33). In using the observed data, it is often desirable that the statistical expectation of the estimated mean equal the actual mean. This is called an unbiased estimate of the mean. The framework for this estimation is to view the spectral image or scene as a collection of  $N$  random pixel vectors. This

implies that the scene is comprised of  $N$  pixel vectors, each consisting of an L-band spectrum. The unbiased estimate of the mean spectrum for the scene is given by:

$$\mathbf{m} = \frac{1}{N} \sum_{j=1}^N \mathbf{x}_j = \begin{bmatrix} \mathbf{m}_1 \\ \vdots \\ \mathbf{m}_L \end{bmatrix} \quad (2.2)$$

where  $\mathbf{x}_j$  represents the spectrum of the  $j^{\text{th}}$  pixel of the scene. The mean spectrum vector,  $\mathbf{m}$ , of Equation 2.2 can also be interpreted as a L-dimensional vector with each component representing the average brightness value over the entire image for one particular band.

The second definition of importance in characterizing random vectors is that of the covariance matrix. The covariance matrix is defined in vector and expanded component form as:

$$\sum_{\mathbf{x}} = \mathbf{E}\{(\mathbf{x} - \mathbf{m})(\mathbf{x} - \mathbf{m})^T\} =$$

$$\begin{bmatrix} \mathbf{E}\{(\mathbf{x}_1 - \mathbf{m}_1)^2\} & \mathbf{E}\{(\mathbf{x}_1 - \mathbf{m}_1)(\mathbf{x}_2 - \mathbf{m}_2)\} & \dots & \mathbf{E}\{(\mathbf{x}_1 - \mathbf{m}_1)(\mathbf{x}_L - \mathbf{m}_L)\} \\ \mathbf{E}\{(\mathbf{x}_2 - \mathbf{m}_2)(\mathbf{x}_1 - \mathbf{m}_1)\} & \mathbf{E}\{(\mathbf{x}_2 - \mathbf{m}_2)^2\} & \dots & \mathbf{E}\{(\mathbf{x}_2 - \mathbf{m}_2)(\mathbf{x}_L - \mathbf{m}_L)\} \\ \vdots & \vdots & \ddots & \vdots \\ \mathbf{E}\{(\mathbf{x}_L - \mathbf{m}_L)(\mathbf{x}_1 - \mathbf{m}_1)\} & \mathbf{E}\{(\mathbf{x}_L - \mathbf{m}_L)(\mathbf{x}_2 - \mathbf{m}_2)\} & \dots & \mathbf{E}\{(\mathbf{x}_L - \mathbf{m}_L)^2\} \end{bmatrix} \quad (2.3)$$

where  $\mathbf{m}$  is the mean vector of the entire image defined in equation 2.2. The covariance matrix is symmetric, and the elements of the main diagonal represent the variances associated with each of the component variables of the random vector  $\mathbf{x}$ . In the case of spectral imagery, the variance is a measure of how the brightness value of a particular band varies over all spatial image pixels and the covariance describes the scatter of pixel points in the principal components vector space.

The covariance matrix is the set of second central moments of the distribution, which are also referred to as moments about the mean since the mean component is subtracted from each random variable. The unbiased estimate of the covariance matrix is generated by:

$$\sum_{\mathbf{x}} = \frac{1}{N-1} \sum_{j=1}^N (\mathbf{x}_j - \mathbf{m})(\mathbf{x}_j - \mathbf{m})^T \quad (2.4)$$

where  $\mathbf{x}_j$  is again the pixel vector associated with the  $j^{\text{th}}$  spatial location (Richards, 1993, p. 134). When the covariance of two random variables is zero, then the random variables are said to be uncorrelated, which implies that these random variables were generated by separate random processes (Leon-Garcia, 1994, p. 337). In the calculation of the unbiased estimates of statistical quantities, the computational expense of the covariance matrix for a large number of samples,  $N$ , must be balanced with the desired degree of accuracy for the estimate. More samples imply better estimates, and in order to ensure sufficient accuracy, the number of samples must be sufficiently large (Fukunaga, 1972, p. 242).

The third statistical definition involves an issue that requires clarification regarding the term “correlation” matrix. In signal processing terminology, the correlation matrix stated as  $E\{\mathbf{xx}^T\}$  is formed exactly as the covariance matrix, except that the mean vector is not subtracted from the random vector  $\mathbf{x}$  (Therrien, 1992, p. 33).

While the correlation matrix is more frequently used in signal processing where zero mean signals are the norm, remote sensing uses the covariance matrix since negative radiance values do not have a clear physical significance.

In statistical and remote sensing applications, the correlation matrix is usually defined in terms of the covariance matrix. The  $ij^{\text{th}}$  element of the statistical version of the correlation matrix is:

$$\rho_{ij} = \frac{\sigma_{ij}}{\sqrt{\sigma_{ii}\sigma_{jj}}} \quad (2.5)$$

where  $\sigma_{ij}$  is an element of the covariance matrix and the covariance between bands  $i$  and  $j$  in  $S_x$ ,  $\sigma_{ii}$  represents the variance of the  $i^{\text{th}}$  band of data, and the square root of variance is defined as the standard deviation (Richards, 1993, p. 135).

The statistical and signal processing versions of correlation do not produce the same matrix. The statistical definition produces a matrix that has a unit main diagonal and can be represented as:

$$\mathbf{R}_x = \begin{bmatrix} 1 & \rho_{12} & \cdots & \rho_{1N} \\ \rho_{21} & 1 & \cdots & \rho_{2N} \\ \vdots & \vdots & \ddots & \vdots \\ \rho_{N1} & \rho_{N2} & \cdots & 1 \end{bmatrix} \quad (2.6)$$

(Searle, 1982, p. 348). Apparently, dividing the covariance matrix elements by their standard deviations has the effect of reducing all the variables to an equal importance since all have unit variance. The signal processing definition does not produce a unit diagonal matrix, though it is symmetric. The off-diagonal elements of  $\mathbf{R}_x$ , represented by  $\rho_{ij}$  are called correlation coefficients. They range between  $-1$  and  $+1$  in value, and provide a measure of how well two random variables vary jointly by quantifying the degree of fit to a linear model (Research Systems, Inc., 1995, p. 20-6). A value near  $+1$  or  $-1$  represents a high degree of fit between the random variables to a positive or negative model, whereas a value near zero implies that the random variables exhibit a poor fit to the linear model. The conclusion that may be drawn is that a high degree of fit implies well-correlated random variables, whereas a correlation coefficient of zero is indicative of statistically orthogonal random variables. We will assume that we are dealing with the statistical definition of the correlation matrix, though a more descriptive term for the “correlation” matrix might be the “normalized” or “standardized” covariance matrix.

The definitions of statistical properties become clearer when they are linked to a physically observable phenomenon. The next few illustrations attempt to show the large amount of information revealed by the statistics of the data. Table 2.1 shows the covariance and correlation matrices for the Landsat data of Canon City (Diersen, 2000, p. 19).

Covariance Matrix for Canon City TM Data						
Band	Band 1	Band 2	Band 3	Band 4	Band 5	Band 6
1	45.391430					
2	54.157121	69.760492				
3	62.472157	79.432844	96.376932			
4	48.824654	64.610172	77.863810	100.500970		
5	48.318837	64.421129	79.247686	74.711596	87.056432	
6	43.826169	57.616349	70.393457	57.981971	70.991722	63.739045

Correlation Matrix for Canon City TM Data						
Band	Band 1	Band 2	Band 3	Band 4	Band 5	Band 6
1	1.000000					
2	0.962418	1.000000				
3	0.944524	0.968744	1.000000			
4	0.722881	0.771633	0.791159	1.000000		
5	0.768651	0.826653	0.865166	0.798735	1.000000	
6	0.814786	0.864049	0.898138	0.724444	0.953025	1.000000

Table 2.1. Covariance and Correlation Matrices of Landsat TM Data.

In examining the Landsat covariance matrix, we see that the highest variance results from band four, the lowest covariance is between bands one and six, and the highest covariance is between bands two and three. The correlation coefficient is highest between bands two and three and is lowest between bands one and four. These statistics can lead to some conclusions. First, band four has more variance, or contrast over the scene, than any other band. Although it can be assumed that this means that band four can detect some sort of unique information better than the other bands, first a point has to be clarified: whether this variance was caused by signal coming from the ground or it was only noise introduced by the sensor or the atmosphere in the particular band. If the signal-to-noise ratio of the sensor in band four is known then the question can be answered. Signal-to-noise ratio (SNR) is the ratio of signal power to noise power, and can be obtained using the variances instead of the power itself. Second, band one exhibits the lowest correlation coefficient when compared to all other bands. Similarly, before an assumption is made that band one detects unique information, the signal-to-noise characteristics of band one must be investigated. For example, if band one consisted purely of noise, then it would exhibit an even lower correlation with other bands, close to zero if not zero proper. This is independent of the other bands, not because it carries any information.

Another means of characterizing the statistics of the data is the scatter plot. The scatter plot visually represents the two-dimensional distribution of pixels selecting two of the available bands. Two band combinations are shown in Figure 2.5. The scatter plot is a representation of all the two-dimensional random pixel vectors formed by the two bands of interest. By plotting the data of one band against that of another, information regarding the statistical similarity of bands may be inferred. The scatter plots for the Landsat image show a definite linear feature when a high correlation coefficient exists, as between bands two and three. Thus, bands two and three are statistically similar, to the extent that there appears to be a near linear relationship between their random variables. The correlation coefficient of 0.9687 substantiates this observation. This is in contrast to the more distributed shape for the scatter plot of band one data versus band four where the correlation coefficient is 0.7229.

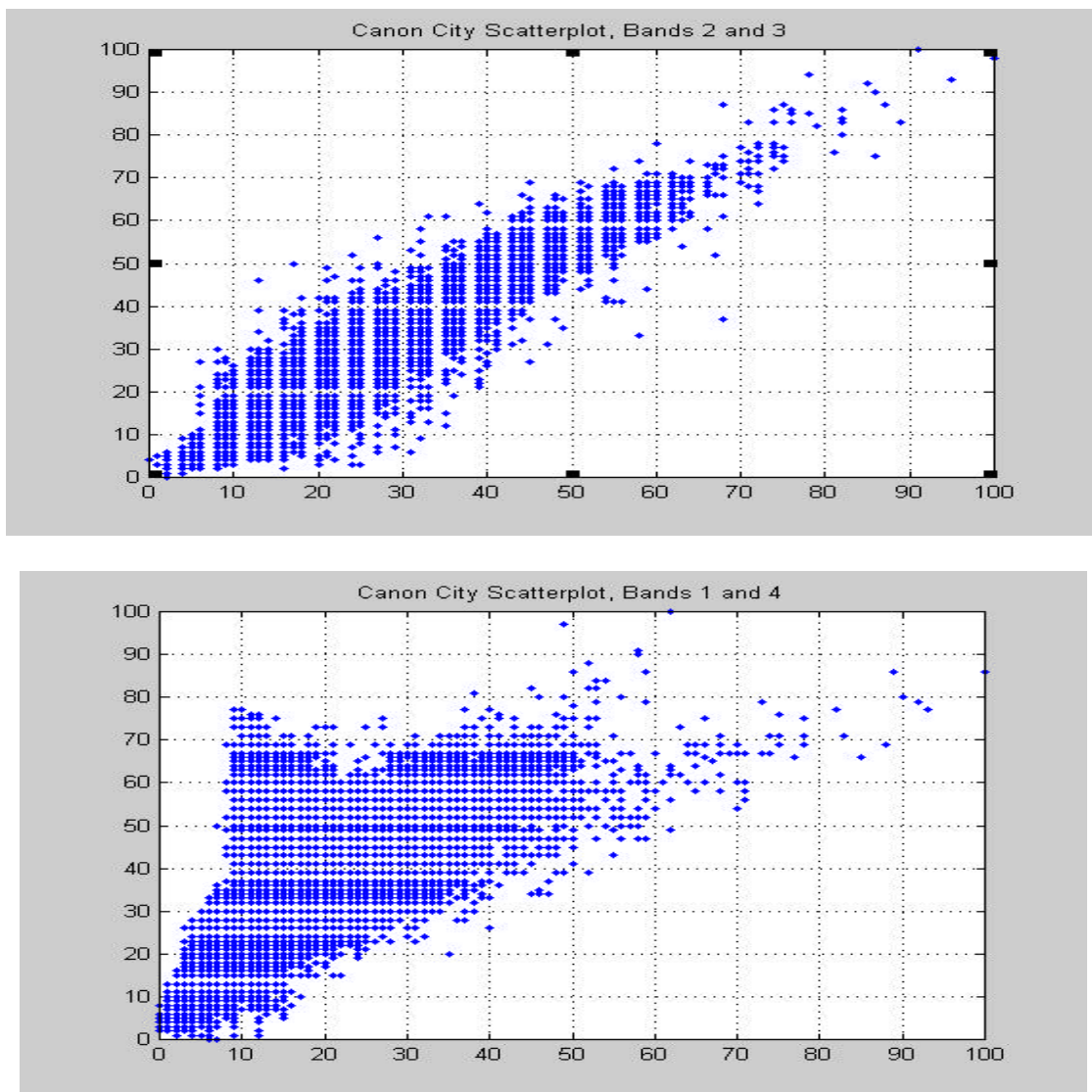


Figure 2.5. Scatter Plots of Canon City Landsat TM Data Showing Highly Correlated (2<sup>nd</sup> & 3<sup>rd</sup>) and Less Correlated (1<sup>st</sup> & 4<sup>th</sup>) Band Combinations.

This graphically depicts the more independent and less correlated nature of the data in band four, as evidenced by the lower correlation coefficient of 0.7229. Groupings of pixels that have the most variance and will form the basis for the studied false-color mapping strategy are clearly shown in the scatter plot.

Another technique used to extract information about the scene is analyzing the plots of various pixel vectors as seen in Figure 2.6. It becomes apparent how the spectrum of the vegetation in a Lake Tahoe scene sharply spikes up at wavelength 700nm whereas

the spectrum of the road in a Davis-Monthan AFB scene remains relatively unchanged. This corresponds to the chlorophyll absorption band edge that occurs at a wavelength of about 700nm. This feature indicates that there are significant differences in the spectral shapes of the observed pixel vectors that start at the particular wavelength. The interpretation lies on the fact that the scene consists of both vegetation and non-vegetation pixel vectors. If the pixel vectors did not possess significantly different shapes, then this feature would not have manifested itself.

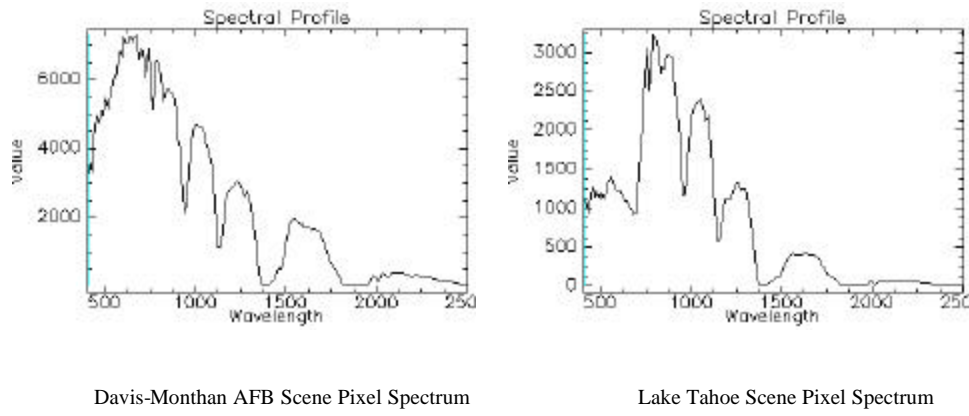


Figure 2.6. Typical Pixel Vectors From Hyperspectral Images.

Although these observations are superficial, they demonstrate how a certain amount of useful information can be derived from the statistics of the scene. A more refined study of scene statistics, such as that pursued by Brower, et. al., (1996), finds that the scene statistics can be used to differentiate urban and rural areas. This idea can be carried further to the problem of differentiating small man-made objects in a natural background but it is beyond the scope of this study. Considered independently, the scene statistics are interesting in that they provide further perspective and understanding into the nature of the scene. It is also important that by preparing the ground for an

understanding of the techniques that use statistics to describe the background, the invariant display problem can be handled more efficiently.

### 3. Related Signal Processing and Linear Algebra Concepts

#### a. *Linear Transformations of Random Variables*

Linear transformations will be used throughout this study as the fundamental basis of the hyperspectral image analysis technique. The statistical definitions of the data using the covariance matrix and its standardized form, the correlation matrix, form the basis for an invariant display strategy. Understanding the effect of a linear transformation on these matrices is also important and will be addressed.

A linear transformation of a vector  $\mathbf{x}$  into a vector  $\mathbf{y}$  is accomplished by the matrix  $\mathbf{A}$  in the relation  $\mathbf{y}=\mathbf{Ax}$ . Figure 2.7 illustrates this concept using two-dimensional vectors.

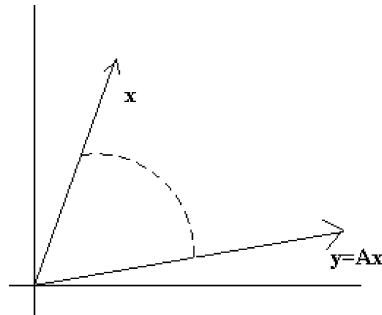


Figure 2.7. Linear Transformation of a Two-dimensional Vector.

The transformation matrix  $\mathbf{A}$  rotates and scales the vector  $\mathbf{x}$  into the new vector  $\mathbf{y}$ . Since second order moment matrices of random vectors are symmetric, we may assume that  $\mathbf{A}$  is symmetric. The expectation operator is linear, which implies that the mean of the random vector  $\mathbf{x}$  is transformed as:

$$E\{\mathbf{y}\}=E\{\mathbf{Ax}\}=\mathbf{AE}\{\mathbf{x}\} \quad (2.7)$$

which can be restated as  $\mathbf{m}_y=\mathbf{Am}_x$ , where the subscript on the mean vector denotes which random vector the mean vector represents. Similarly, using the definition of the second

order moment, the covariance matrix is transformed by the matrix  $\mathbf{A}$  so that (Therrien, 1992, p.45)

$$\sum_y = \mathbf{A} \sum_x \mathbf{A}^T \quad (2.8)$$

A particularly useful transformation is one which transforms a random vector  $\mathbf{x}$  into another random vector  $\mathbf{y}$  whose  $k^{th}$  and  $l^{th}$  components have the property of statistical orthogonality such that (Therrien, 1992, p.50):

$$E\{\mathbf{y}_k \mathbf{y}_l\} = 0 \quad k \neq l. \quad (2.9)$$

The statistically orthogonal or uncorrelated random variables that result from such a transformation cause the transformed data covariance matrix to be diagonal. The means of achieving such a transformation that diagonalizes the covariance matrix is provided by the concept of eigenvectors and eigenvalues.

### *b. Eigenvectors and Eigenvalues*

The eigenvalues of a  $L \times L$  matrix  $\mathbf{A}$  are the scalar roots of its characteristic equation, and are denoted as  $\{\lambda_1, \dots, \lambda_L\}$ . The nonzero vectors  $\{\mathbf{e}_1, \dots, \mathbf{e}_L\}$ , which satisfy the equation

$$\mathbf{A}\mathbf{e}_k = \lambda_k \mathbf{e}_k \quad (2.10)$$

are called the eigenvectors of  $\mathbf{A}$ . An eigenvector defines a one-dimensional subspace that is invariant with respect to premultiplication by  $\mathbf{A}$  (Golub and Van Loan, 1983, p. 190). In applying the above definitions of the eigenvalue and eigenvector to the  $L \times L$  covariance matrix, we obtain

$$\sum_x \mathbf{e}_k = \lambda_k \mathbf{e}_k. \quad (2.11)$$

The covariance matrix in this relation may be viewed as a linear transformation that maps the eigenvector  $\mathbf{e}_k$  into a scaled version of itself (Therrien, 1992, p. 50). Because of the symmetry of the real covariance matrix, the  $L$  eigenvalues are guaranteed to be non-negative and real (Searle, 1982). It is also possible to find  $L$  orthonormal eigenvectors  $\{\mathbf{e}_1, \dots, \mathbf{e}_L\}$ , that correspond to the  $L$  eigenvalues (Therrien, 1992, p. 50) that satisfy

$$\mathbf{e}_i^T \mathbf{e}_j = \delta_{ij}. \quad (2.12)$$

*c. Unitary Transformations*

Suppose that the eigenvectors of the  $L \times L$  covariance matrix  $S_x$  are packed into a matrix  $\mathbf{E}$  as column vectors. Then, because of the orthonormality of the eigenvectors, the matrix  $\mathbf{E}$  transforms the covariance matrix in the following manner:

$$\mathbf{E}^T \sum_x \mathbf{E} = \begin{bmatrix} \leftarrow \mathbf{e}_1^T \rightarrow \\ \vdots \\ \leftarrow \mathbf{e}_\ell^T \rightarrow \end{bmatrix} \sum_x \begin{bmatrix} \uparrow & & \uparrow \\ \mathbf{e}_1 & \cdots & \mathbf{e}_\ell \\ \downarrow & & \downarrow \end{bmatrix} = \begin{bmatrix} \lambda_1 & & \mathbf{0} \\ & \ddots & \\ \mathbf{0} & & \lambda_\ell \end{bmatrix} = \Lambda, \quad (2.13)$$

following the rules of linear transformations (Therrien, 1992, p. 45). The transformation matrix  $\mathbf{E}^T$  defines a linear transformation of a random vector  $x$  into a random vector  $y$ , by the relation

$$y = \mathbf{E}^T x \quad (2.14)$$

in which the covariance matrix of  $y$  is a diagonal matrix represented by  $\Lambda$ . This diagonalization of the covariance matrix  $S_x$  is another way of stating that the components of random vector  $y$  are now uncorrelated since all off-diagonal elements of  $\Lambda$  are zero. The orthonormal columns of  $\mathbf{E}$  imply that the transformation matrix  $\mathbf{E}^T$  represents a unitary transformation defined by (Therrien, 1992, p. 51)

$$\mathbf{E}^T \mathbf{E} = \mathbf{E} \mathbf{E}^T = \mathbf{I} \quad (2.15)$$

*d. A Geometric Interpretation of the Unitary Transform*

If we assume that the data has a Gaussian distribution, then we can describe its probability density function (pdf) with a family of ellipsoids as:

$$(\mathbf{x} - \mathbf{m}_x)^T \sum_x^{-1} (\mathbf{x} - \mathbf{m}_x) = \text{const tan } t \quad (2.16)$$

Since the matrix  $\mathbf{E}$  is orthonormal, the implication is that the eigenvectors of  $S_x$  are the same as those of its inverse, and the eigenvalues of  $S_x^{-1}$  are simply the reciprocals of those of  $S_x$  (Jolliffe, 1986, p. 14). Thus, the inverse transformation may be written as

$$\mathbf{x} = \mathbf{E}^T \mathbf{y} \quad (2.17)$$

and the equation defining the contours of constant density may be rewritten as:

$$(\mathbf{x} - \mathbf{m}_x)^T \mathbf{E} \Lambda^{-1} \mathbf{E}^T (\mathbf{x} - \mathbf{m}_x) = (\mathbf{y} - \mathbf{m}_y)^T \Lambda^{-1} (\mathbf{y} - \mathbf{m}_y) = \sum_{k=1}^{\ell} \frac{|\mathbf{y}_k - \mathbf{m}_k| |\mathbf{y}_k - \mathbf{m}_k|}{\lambda_k} = \text{const.} \quad (2.18)$$

which is the equation for an ellipse with the principal axes of the ellipse being aligned with the eigenvectors and the magnitudes proportional to  $\lambda_k^{1/2}$  (Jolliffe, 1986, p. 19). This geometrically illustrates the role that eigenvalues and eigenvectors play in the unitary transform. Figure 2.8 shows that the unitary transformation is equivalent to a rotation of the coordinate axes.

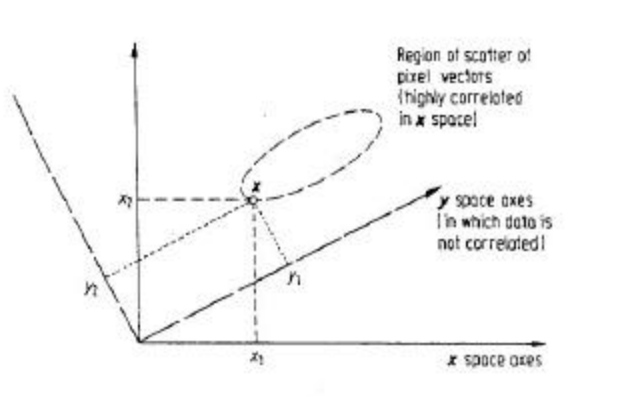


Figure 2.8. The Unitary Transformation as a Rotation of Axes. From Richards, 1993.

The tilt of the ellipse with respect to the original coordinate system is indicative of the fact that correlation exists between the original vector components (Therrien, 1992, p. 59). In the new coordinate system defined by the unitary transformation, the axes of the ellipse are parallel to the new axes, showing that the vector components are indeed uncorrelated in the coordinate system. Although the assumption was made that the data was Gaussian, this concept of two-dimensional ellipsoids is a useful one in understanding the workings of the transformation even for non-Gaussian data. In this context, the scatter plots of the Landsat data are useful in portraying a rough idea of the distribution of the probability density function of the random vectors.

## 4. Principal Components Analysis

### a. General

In spectral imagery high correlation is observed between adjacent bands. The spectral overlap of the sensors and the wide frequency range of the energy reflected from the ground account for this high correlation (Rao and Bhargava, 1996, p. 385). The resulting redundancy observed in the data, therefore, needs to be removed. In order to maximize the spectral variability in hyperspectral remote sensing, an analytical technique called Principal Component Analysis (PCA) is used. It is based on the linear transformation of the observed axes to a new coordinate system. This unitary transformation is graphically depicted in Figure 2.9 as operating on observed pixel vectors to produce new pixel vectors with uncorrelated components. The principal components transformation decorrelates the information in the original bands and allows the significant information content of the scene to be represented by a smaller number of linear combinations of the original bands called principal components.

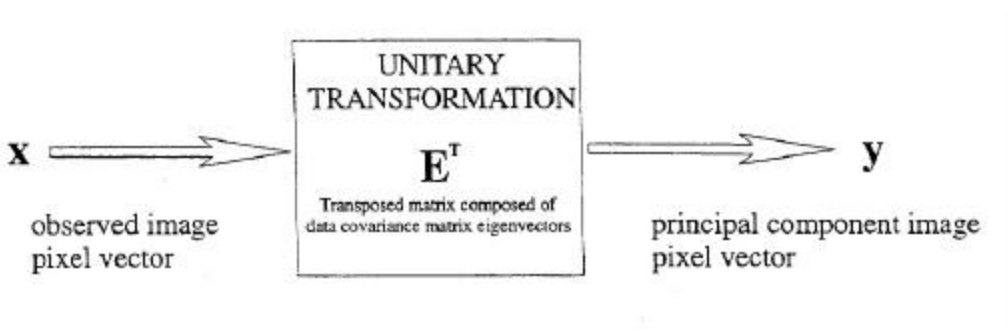


Figure 2.9. PC Transformation Depicted as a Linear Transformation.

Since PCA methods are largely based on the statistics of the observed variables, requiring no *a priori* deterministic information about the variables in the image, they are of considerable interest in developing an invariant display strategy. Therefore a methodology can be developed where no preprocessing needs to be performed prior to displaying the data utilizing “global” *a priori* knowledge.

**b. Background**

Statistics and linear algebra are the fields where the PCA idea originated.

The mathematical underpinnings of PCA deal with the diagonalization of the covariance matrix via eigendecomposition of the data by unitary transform and serves as a bridge between matrix algebra and stochastic processes (Haykin, 1996). The wide applicability of PCA is due to the fact that it assumes a stochastic outlook of the data, which is fundamental to the analysis of data in many scientific disciplines. The views of two disciplines which employ PCA will be investigated in order to better visualize some of the mechanics of this seemingly simple transformation. The two views are those of multivariate data analysis and signal processing. The reason behind the preference for the use of this technique in remotely sensed imagery analysis, in general, and particularly in an invariant display strategy, will be better understood through the presentation of the ideas that motivate the PCA.

(1) Multivariate Data Analysis View. PCA was described by Pearson in 1901 and introduced as the Hotelling transform in 1933 by Hotelling for application in educational psychology (Singh and Harrison, 1985, p. 884). Hotelling's goal was to find a fundamental set of independent variables of smaller dimensionality than the observations that could be used to determine the underlying nature of the observed variables (Hotelling, 1933, p. 417). In many scientific experiments, the large number of variables makes the problem of determining the relative importance of specific variables intractable. Hotelling's method makes the problem manageable by discarding the linear combinations of variables with small variances, and studying only those linear combinations with large variances. Since the important information in the data is usually contained in the deviation of the variables from a mean value, it is logical to seek a transform which provides a convenient means of identifying the combinations of variables most responsible for the variances (Anderson, 1984, p. 451). The linear combinations of the original variables which behave sufficiently similarly are combined into new variables called principal components. In this context, principal components analysis studies the covariance relationships within a data set by investigating the number of independent variables, and identifies the natural associations of the variables.

Mathematically represented, each principal component is a scalar formed by a linear combination of the elements of the observed random vector  $\mathbf{x}$ , where each vector component corresponds to a random variable. The principal components are constructed in such a manner as to be uncorrelated with all other principal components and ordered so that variance is maximized (Jolliffe, 1986, p. 2). The  $k^{\text{th}}$  principal component is obtained by multiplying the transposed  $k^{\text{th}}$  eigenvector of  $\mathbf{S}_x$  by the data vector  $\mathbf{x}$ , as depicted in the equation

$$\mathbf{y}_k = \mathbf{e}_k^T \mathbf{x}. \quad (2.19)$$

The  $k^{\text{th}}$  principal component is also called a score, and the components of the eigenvector are called loadings because they determine the contribution of each original variable to the principal component. Generalizing the scalar result of Equation 2.19 to a vector result:

$$\mathbf{y} = \mathbf{E}^T \mathbf{x} \quad (2.20)$$

a vector of  $L$  principal components is obtained when the product of all the transposed eigenvectors of  $\mathbf{S}_x$  and the data vector,  $\mathbf{x}$  are taken.

While the property of the unitary transform to produce new uncorrelated variables has been previously discussed, the property of the unitary transform to maximize the variance, which is central to the PCA, will be discussed further. The best illustration of this property is the algebraic derivation of the PCA. The goal is to maximize the variance of the first principal component, denoted as  $\text{VAR}[y_1]$  or  $\text{VAR}[\mathbf{e}_1^T \mathbf{x}]$ . By the definition of variance as a second order moment, this is equivalent to maximizing  $\mathbf{e}_1^T \mathbf{S}_x \mathbf{e}_1$ , where the eigenvectors are orthonormal, so that  $\mathbf{e}_1^T \mathbf{e}_1 = 1$ . The method of Lagrange multipliers is employed so that the expression to be maximized is differentiated with respect to the eigenvector and set equal to zero as

$$\frac{\partial}{\partial \mathbf{e}_1} [\mathbf{e}_1^T \sum_x \mathbf{e}_1 - \lambda (\mathbf{e}_1^T \mathbf{e}_1 - 1)] = \mathbf{0} \Rightarrow (\sum_x - \lambda \mathbf{I}) \mathbf{e}_1 = \mathbf{0} \quad (2.21)$$

In Equation 2.21,  $\lambda$  is a Lagrangian multiplier in the left hand expression and corresponds to the largest eigenvalue of  $\mathbf{S}_x$  in the right hand expression, and  $\mathbf{e}_1$  is the eigenvector corresponding to the largest eigenvalue (Jolliffe, 1986, p. 4). Thus, the eigenvalues of  $\mathbf{S}_x$  represent the variances of the principal components, and are ordered

from largest to smallest magnitude. If the original variables have significant linear intercorrelations, as spectral imagery does, then the first few principal components account for a large part of the total variance. (Singh and Harrison, 1985, p. 883).

(2) Signal Processing View. In the analysis of random signals, the key is to have a set of basis functions that make the components of the signal statistically orthogonal or uncorrelated (Therrien, 1992, p.173). The Karhunen-Loeve Transform (KLT) was introduced in 1947 for the analysis of continuous random processes, and is developed here in its discrete form, the DKLT. It is the same unitary transform previously presented, but is posed to solve the problem from a different perspective. The motivation for the DKLT is actually an expansion, best seen in Figure 2.10, which shows a discrete observed signal as a weighted sum of basis functions, which are in fact the eigenvectors of the covariance matrix. The observed pixel vector spectrum may be thought of as a discrete signal, indicated by the square brackets in the notation of Figure 2.10.

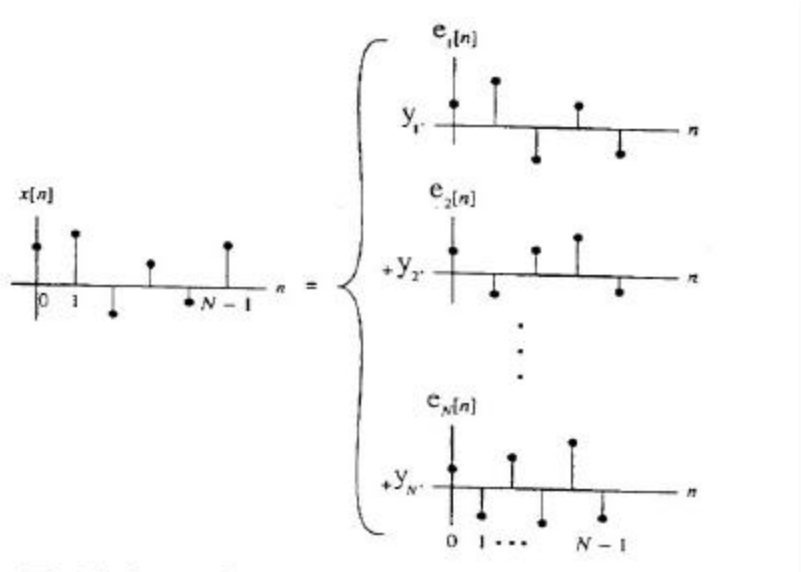


Figure 2.10. The Karhunen-Loeve Expansion in Terms of Discrete Signals. After Therrien, 1992.

Whereas in the PCA approach the original variables are weighted by eigenvector components to form principal components, in the DKLT the eigenvector basis functions,  $\{e_1, \dots, e_N\}$ , are weighted by the principal component scores,  $\{y_1, \dots, y_N\}$ ,

to form a representation of the observation. The DKLT has an optimal representation property in that it is the most efficient representation of the observed random process if the expansion is truncated to use fewer than  $N$  orthonormal basis functions. This makes it very attractive from a compression perspective, and explains the popularity of DKLT as a compression scheme.

Another important property associated with the DKLT is the equivalence between the total variance in the vector  $\mathbf{x}$  and the sum of the associated eigenvalues. This property is mathematically stated by the equation

$$\sum_{i=1}^L \sigma_i^2 = \sum_{i=1}^L \lambda_i \quad (2.22)$$

In equation 2.22,  $\sigma_i^2$  is the variance of the original variables and  $\lambda_i$  is the eigenvalue representing the variances of the transformed variables and the index  $i$  ranges over all  $L$  bands. This property only holds for the orthonormal vectors that are eigenvectors of  $Sx$  and not for other orthonormal basis sets of vectors (Kapur, 1989, p. 501).

When a representation of a signal is formed by using fewer than  $L$  basis functions, the mean square error (MSE) is a means of quantifying how well the representation corresponds to the original signal by measuring the power of the difference between the representation and original signals. The MSE incurred by truncating the representation is equal to the sum of the eigenvalues of the covariance matrix that were left out of the representation (Therrien, 1992, p. 179). Conversely, the largest eigenvalues and their corresponding eigenvectors can be used to represent the inherent dimensionality of the signal. This corresponds to the number of dimensions that would be needed to represent the signal to some predetermined MSE.

In signal processing applications, the DKLT is a means of compressing data by representing it with a truncated number of eigenvectors. It is also an optimum way of detecting a signal in noise and works particularly well for the detection of narrowband signals. Since a significant portion of the signal energy lies in the direction of the first few eigenvectors, those eigenvectors can be said to define a subspace for the signal and all other eigenvectors define the subspace for the noise. This simple

example is the basis for several high resolution methods of spectral estimation used to detect sinusoids in noise (Scharf, 1991, p. 483).

### *c. Operation*

PCA uses the eigenvectors of  $S_x$  to assemble a unitary transformation matrix which, when applied to each pixel vector, transforms the original pixel vector into a new vector with uncorrelated components ordered by variance. The eigenvector components act as weights in the linear combination of the original band brightness values that form the principal components (Richards, 1993). The new image associated with each eigenvector is referred to as the principal component image. The principal component images are ordered from largest to smallest in terms of variance, and are revealing in their composition. It must be kept in mind that the PCA is an exploratory technique that constructs new variables called the principal components (PCs) (Singh and Harrison, 1985). These new variables are artificial and do not necessarily have a physical meaning, as they represent linear combinations of the observed variables and cannot themselves be observed directly, but they should be related because the first eigenvector in spectral imaging is a representation of the mean solar energy of the scene and the next few eigenvectors deviate as the variance changes.

In traditional application of PCA, the hope is that the transformation will enhance the contrast of the image by grouping like areas together to such an extent that objects or areas of interest can be more readily discriminated in the principal component images. Jenson and Waltz (1979) give an analogy that clearly explains the role of PCA in the traditional application. They imagine a tube filled with ping-pong balls. Looking at the tube directly from an end, only one ball is apparent, the same way that the original spectral image is. Turning the tube sideways, all of the balls become visible (Jenson and Waltz, 1979, p. 341). PCA has the effect of decorrelating the data so that independent sources of spectral features can be discerned.

Though PCA assumes no *a priori* knowledge of the scene, PCA as described here depends essentially on the scene because scene-specific features will determine the shape of the eigenvalues. Nevertheless, certain general observations can be made regarding the PCA and an associated physical meaning without any knowledge of the scene. The following figure highlights these observations. Figure 2.11 shows the first

20 PC images of the Lake Tahoe HYDICE scene. For a non-negative symmetric matrix, the first eigenvector is all positive. A weighted sum loosely corresponds to the average spectral radiance. All other eigenvectors must have at least one sign change to be orthogonal to the first eigenvector. This is due to the fact that in forming the first principal component image, the first eigenvector has heavily weighted the original bands possessing the most variance. Thus, the first principal component image will have a variance that is larger than that of any single original band image. It is the weighted sum of the overall response level in all original band images. The second principal component image is the difference between certain original band images. As the principal component image number increases, the PC image holds less of the data variance. This effect manifests itself as a rough decrease in image quality with increasing PC image number.

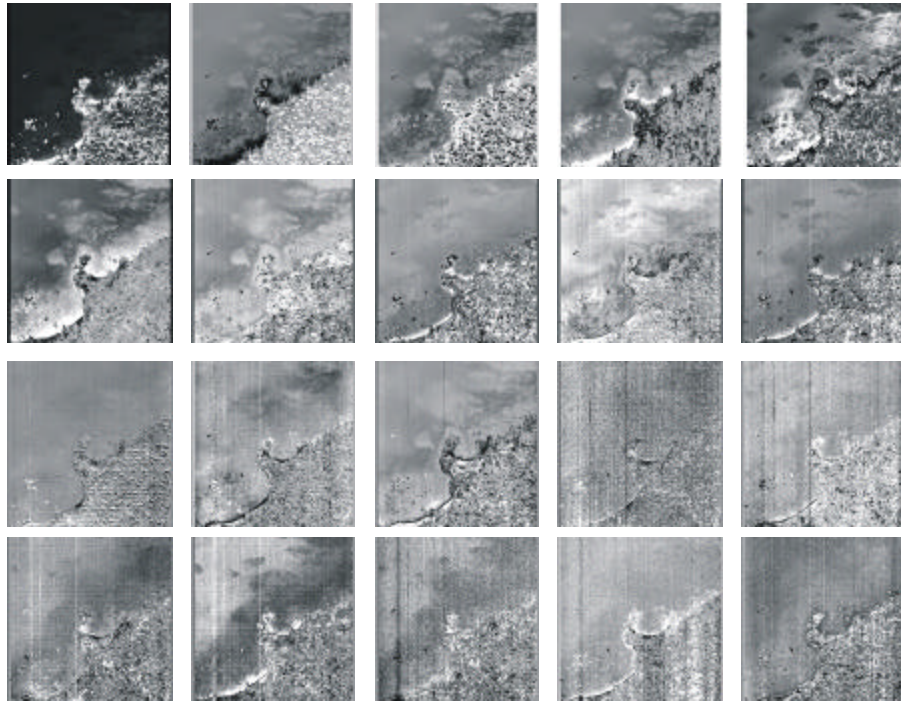


Figure 2.11. First 20 PC Images of Lake Tahoe.

In Figure 2.11, the fact that the first twelve PC images contain relatively clear details of the scene indicates that these PC images together account for the majority of the overall spectral variance in the scene. It is interesting to note that when using PCA, the higher numbered PC images sometimes contain a large amount of local detail. Though it is tempting to dismiss the higher numbered PC images as not containing any

useful information because they have low variance, one must keep in mind that the covariance matrix on which PCA is based is a global measure of the variability of the original image (Richards, 1986, p. 138). This implies that small areas of local detail will not appear until higher PC images since they do not make a statistically significant impact on the covariance matrix. Another point that is noteworthy is the issue of SNR. PCA orders PC images based on total variability. It does not differentiate between the variability representing desirable information and the variability representing undesirable noise (Jenson and Waltz, 1979, p. 338). Ready and Wintz (1973) argue that PCA improves the SNR of the spectral image. Their definition of noise is additive white Gaussian noise with a variance of  $s_n^2$ . The SNR of the original image is

$$(\text{SNR})_x = \frac{\sigma_{x_{max}}^2}{\sigma_n^2} \quad (2.23)$$

which is the maximum original band variance over the noise variance. The SNR of the PC images is

$$(\text{SNR})_y = \frac{\lambda_1}{\sigma_n^2} \quad (2.24)$$

which is the largest eigenvalue (or new variance) over the noise variance. Since the first eigenvalue always has a greater variance than any of the original bands, the improvement in SNR is

$$\Delta \text{SNR} = \frac{(\text{SNR})_y}{(\text{SNR})_x} = \frac{\lambda_1}{\sigma_{x_{max}}^2} \quad (2.25)$$

and will be greater than one. The SNR improvement applies as long as the variance of the eigenvalue exceeds that of the original bands. The diminishing SNR manifests itself in Figure 2.11 as an increased fuzziness of the image that begins to appear around the ninth PC image.

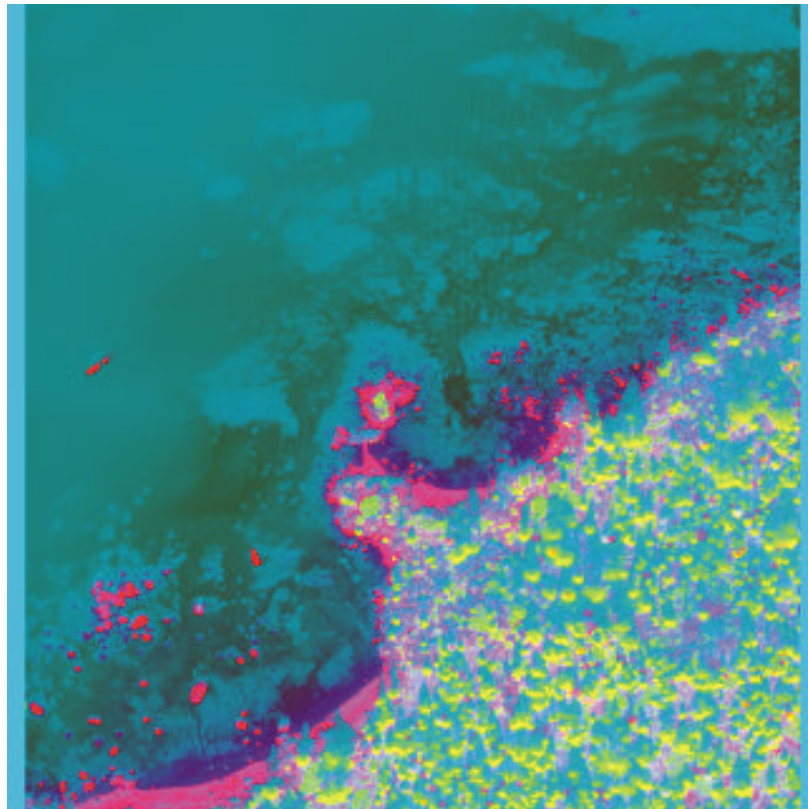


Figure 2.12. Lake Tahoe False Color Image.

A traditional means of presenting PCA images is to form a false color composite image consisting of the first, second, and third PC images as the red, green, and blue colors. Figure 2.12 presents such false color image for the Lake Tahoe scene. This mode of presentation captures the major sources of spectral variability in one image. The levels of detail and contrast apparent in the composite image are interesting to compare with the original image shown in Figure 2.13.



Figure 2.13. Original Lake Tahoe Image in Visible Spectrum.

An aspect of PCA, rarely mentioned in the related on PCA literature, is the characterization of the original and PC images using the behavior of the eigenvalues and eigenvectors. These attributes form an important part of analyzing the scene information content. In spectral images, the typical trend in the eigenvalue magnitude is that a very small number of eigenvalues have a disproportionately large magnitude compared to the others. The obvious reason for this distinct grouping of eigenvalues is that the data in the original image exhibits a high degree of interband correlation and the magnitude of the eigenvalues reflects the degree of redundancy in the data (Richards, 1986, p. 137). Phrased another way, the inherent dimensionality, which is represented by the number of large eigenvalues of the data, is much smaller than the original number of dimensions. From a compression view this is good, since the image variance will be accounted for by a very small number of principal components. From a strict analysis viewpoint, it does not reveal as much information. If the problem were that of a narrowband signal embedded in noise, then the large eigenvalues would be associated with the signal. In the hyperspectral imagery analysis problem, the spectrum associated with a target is not

narrowband, and therefore it is not clearly delineated from the eigenvalues of the background and other interfering signatures. The eigenvalues can be divided into a primary and a secondary set, where the secondary set roughly corresponds to the effects of instrumentation noise (Smith, Johnson, and Adams, 1985, p. C798). The primary set corresponds to the linear combinations of original bands that cause the most variance in the scene. The quality of the first eight PC images noted in Figure 2.11 corresponds to the steeper initial slope of the detailed eigenvalue plot. The above results clearly indicate that the variance for the transformed data are concentrated in the first few PC bands, indicating that the dimensionality is on the order of 10 instead of 210. It is important to note that the variance of the original data is equal to that of the transformed data. This property shows that the PC transformation simply redistributes the concentration of variance in the bands of a spectral image so that the higher variances occur in the first PC bands (Stefanou, 1997).

The eigenvector behavior is less clear than that of the eigenvalues. The eigenvectors form the bases of the principal components subspaces. Physically, the eigenvectors correspond to the principal independent sources of spectral variation. As such, the wavelengths at which the maxima and the minima of the eigenvectors occur account for the wavelengths that contribute the most to a particular independent axis of variation (Smith, Johnson, and Adams, 1985, p. C808). A signal processing interpretation of the eigenvectors is that the eigenvectors act as band pass filters that transform an input observed spectrum into a new spectrum that has fewer data points (Smith, Johnson, and Adams, 1985, p. C808). This interpretation is comparable to the optimum representation property of the DKLT. Further examination of eigenvector behavior emphasizes the correlation between the eigenvectors and variance occurring in the original image bands and it can be shown that the eigenvectors of the PC transform tend to emphasize those original bands that contain the most variance with larger weights and inclusion in the low numbered eigenvectors (Stefanou, 1997).

The PCA technique has been examined from the perspective of its results and the significance of its inner workings. Key points in PCA analysis are:

-In general, PCA provides an analysis of the data, which guarantees an output set of images ordered by variance.

-Assuming white noise, it improves the SNR in the transformation from the original image cube to the PC images.

-The PC images highlight spectral regions of high variance. However, an area of local detail may not be highlighted by a PC image due to its statistical insignificance.

-PCA does not differentiate between noise and signal variances because it operates strictly on the variance of the observed data.

Concerning the implementation of PCA, it has to be noted that the computation of the eigenvectors and eigenvalues of  $S_x$  is an expensive operation. Specific methods from computational linear algebra such as inverse iteration, QR factorization, and singular value decomposition (SVD) are all applicable in their calculation (Watkins, 1991).

The previous discussion highlights three crucial issues in development of an invariant display strategy utilizing principal components. The first issue is the fact that PC band number one is typically a representation of the scene average brightness and is generally dominated by solar radiance, but major scene constituents such as water and vegetation in the Tahoe scene can affect it. The second issue is that the PC transformation outputs a set of images ordered by variance with the 2<sup>nd</sup>, 3<sup>rd</sup>, ..., N<sup>th</sup> PCs dependent on the specific contents of the image and the third issue is that PCA is sensitive to scaling of the data to which it applied.

## 5. Color Vision

### a. Description

An average human can perceive light radiated at wavelengths ranging between less than 400 nanometers for violet to more than 700 nanometers for red. The detected light bandwidth is perceived as a smoothly varying rainbow of colors, called visible spectrum.

The structure of the human eye resembles that of a camera, featuring the lens and the iris diaphragm as well as the photosensitive layer of the retina covering the

inner wall at the backside of the eyeball. However, while a photographic film presents a relatively constant resolution and spectral sensitivity throughout its exposed surface, the human eye presents a wide variety of performance and capabilities. The human eye apart from its ability to perceive motion in a wide angle and in a wide variety of illumination levels, it has also the ability to detect variations of light and colors utilizing photoreceptive cells located at the retina. These nerve cells are called rods and cones and cover the majority of the eye's interior surface, hence the very wide angle of the human peripheral vision. A cross section of the human eye is illustrated in Figure 2.14.

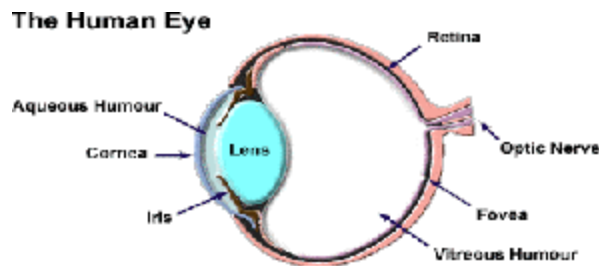


Figure 2.14. Cross Section of the Human Eye.

While the rods in the retina are long and slender and more sensitive to light, the cones are shorter and thicker exhibiting less sensitivity to the light. In Figure 2.15 the relative sensitivity of rods and cones is shown as a function of illumination wavelength.

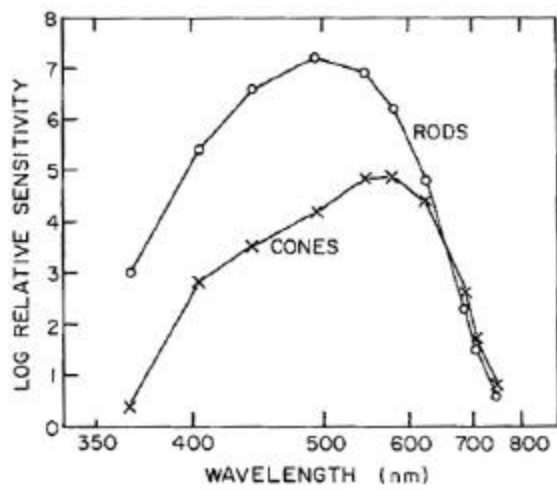


Figure 2.15. Sensitivity of Rods and Cones (Pratt, 1991).

It has been experimentally determined that there are three basic types of cones in the retina (Wald, 1964). These cones have different absorption characteristics as a function of wavelength with peak absorptions in the red (580 nm), green (540 nm) and blue (450 nm) visible spectrum. The combination of the cones excited and the level of their excitation determine our perception of color. Figure 2.16 illustrates the spectral sensitivity of the typical human visual system. The RGB sensors are denoted with the Greek letters  $\rho$  (rho for red),  $\gamma$  (gamma for green) and  $\beta$  (beta for blue). Human vision is especially sensitive to low ambient illumination conditions. The contribution of the cones is little or none in low illumination conditions and primarily the rods accomplish light perception.

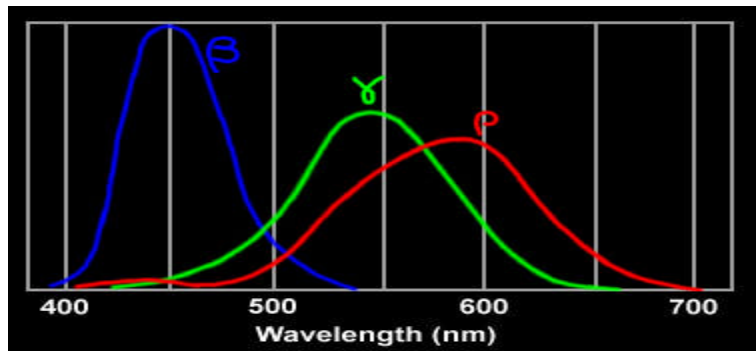


Figure 2.16. Spectral Absorption Curves (Scott, 1997).

The sensitivity curves of the Rho, Gamma and Beta sensors in the human eye determine the intensity of the colors perceived for each wavelength in the visible spectrum. An approximate illustration of the visible spectrum adjusted for the sensitivity curves of all three kinds of sensors is depicted in Figure 2.17.

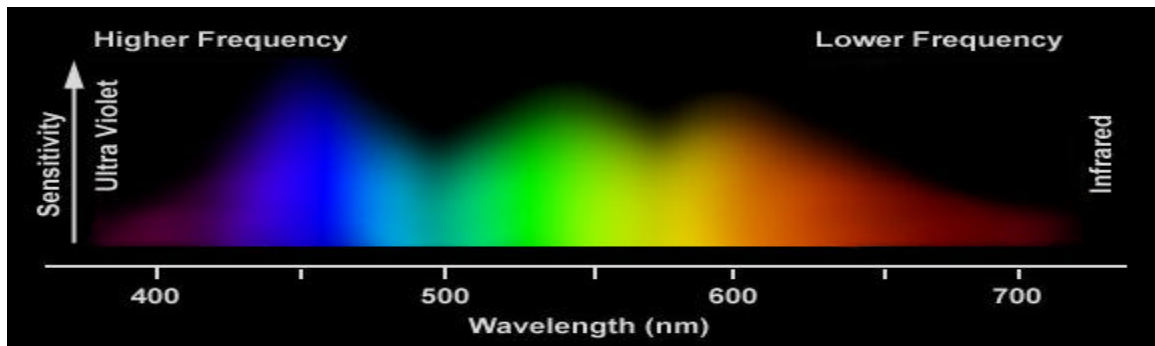


Figure 2.17. Human Visual Spectrum (Scott, 1997).

There are three perceptual definitions of light: brightness, hue, and saturation. If we observe two light sources with the same general spectral shape, the source with the greater intensity will generally appear to be perceptually brighter. Hue is the attribute that distinguishes a red color from a blue color or a violet color. Saturation is the attribute that distinguishes a spectral light from a pastel light within the same hue.

**b. Comparison to Principal Components**

Processing of color within the human eye is accomplished through an achromatic channel and two opponent-color channels. The opponent-color channels are the red-green opponent and the blue-yellow opponent channel (Wyszecki and Stiles, 1967; Buschbaum and Gottschalk, 1983). The A, R-G, and B-Y channels are formed from a principal components analysis, are statistically uncorrelated, and therefore make up orthogonal dimensions in a 3-D color space. Furthermore, it has been shown that there are two fundamental axes within color space comprised of a R-G plane where all colors have an absence of yellowness or blueness and a B-Y plane where all colors have an absence of redness or greenness. The intersection of these two planes is a line with absence of all color, or a gray line, which corresponds to the achromatic channel (Krauskopf, et al., 1982).

We can use the concept of three orthogonal axes to develop the hue, saturation, and value (H-S-V) color representation system. From the previous section, hue indicates a particular color, e.g. the perceived colors of red, green, blue, etc., saturation indicates the purity of a particular hue, e.g.  $S=1$  denotes a pure hue while  $S=0$  denotes absence of color (gray), and value is related to the brightness or intensity of a particular color. The perceptual color space therefore makes up a cone, with the A axis as the axis of rotation of the cone and the R-G and B-Y axes transverse. Hue is determined by computing an angle in the R-G/B-Y plane, and saturation is determined by the angle between a particular point in color space and the gray axis. A graphic representation of this concept is shown in Figure 2.18.

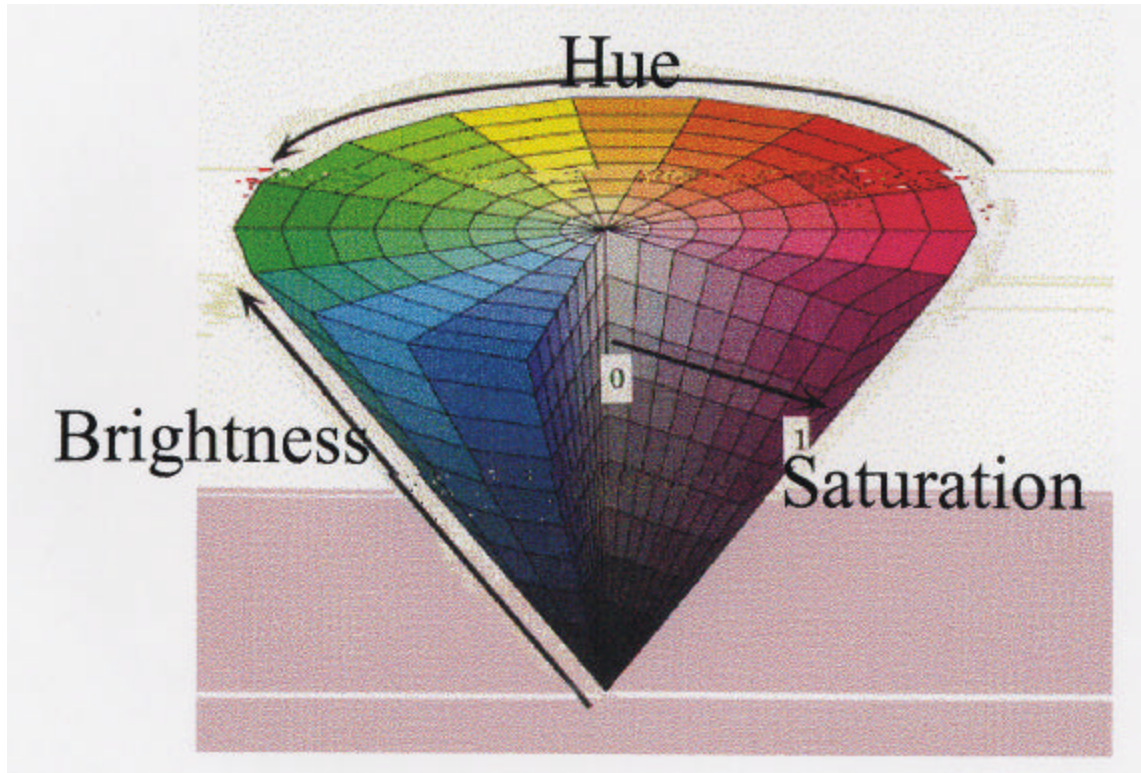


Figure 2.18. Conical Colorspace.

When mapping color space we encounter four distinct problems. The first is that color space is nonlinear. The non-linearity is related to the spectral response functions of the individual photoreceptors. The second problem is that we typically map red next to violet when they actually appear at opposite ends of the spectrum. The third problem consists of the fact that as intensity is increased, the hue is perceived to shift, and this is the issue of color constancy (Brainard, et al., 1993, pp. 165-170). The fourth problem is associated with the color planes. It has been demonstrated that while red-green and blue-yellow planes exist, other similar color-opponent planes do not seem to exist, hence the term “cardinal directions” used by Krauskopf, et al. This cardinal direction scheme will be utilized for the invariant mapping strategy in later sections.

THIS PAGE INTENTIONALLY LEFT BLANK

### III. MAPPING STRATEGY

#### A. PSEUDOCOLOR AND OPPONENT COLOR MAPPING STRATEGIES

In the past, pseudocolor displays have utilized a mapping strategy whereby the principal components were directly depicted by mapping the PCs as follows:

**P1 ? Red,**

**P2 ? Green,**

**P3 ? Blue,**

or

**P1 ? Brightness,**

**P2 ? Hue,**

**P3 ? Saturation.**

Figure 3.1 is a mapping of the first three PCs into (R,G,B) from the Davis-Monthan AFB scene. Although this method does depict some of the high spatial frequency information, much of it is suppressed and there is an apparent smearing, which is a result of how the observer views the data. These methods are not a good fit to human vision.

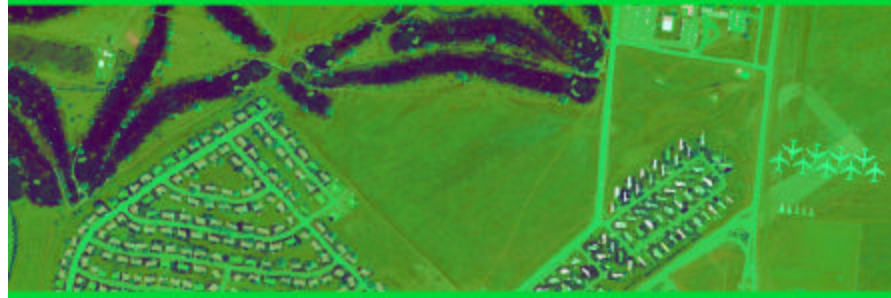


Figure 3.1. Pseudocolor Representation of Davis-Monthan Scene Obtained by Mapping the First Three PCs into (R, G, B).

It has been shown that for humans, the achromatic spectral channel accounts for approximately 97% of color vision, while the R-G and B-Y channels account for approximately 2% and 1% respectively (Buchsbaum and Gottschalk, 1983). From the previous discussion of the principal components transformation, it can be readily seen that the first principal component of a spatial image is roughly achromatic in that it samples the mean illumination distribution and can therefore be reviewed as the intensity or brightness of a hyperspectral image. Continuing along this reasoning, we note that the

second and third PCs contain significantly less scene variance and subsequently higher PCs contain even lower amounts. From this we may be able to conclude that we can map the second and third principal components into the R-G/B-Y plane.

Mapping the first PC into the achromatic channel, the value of the second PC into the R-G channel and the value of the third PC into the B-Y channel yields

$$\begin{aligned} \theta = \text{atan}\left(\frac{\mathbf{P}_3}{\mathbf{P}_2}\right) &\rightarrow \mathbf{H}(\text{Hue}) \\ \frac{\sqrt{\mathbf{P}_2^2 + \mathbf{P}_3^2}}{\mathbf{P}_1} &\rightarrow \mathbf{S}(\text{Saturation}) \\ \mathbf{P}_1 &\rightarrow \mathbf{V}(\text{Value}) \end{aligned} \quad (3.1)$$

where  $P_i$  is the  $i$ th PC (Tyo, et al., 2000).

The mapping of the same Davis-Monthan scene with Equation 3.1 yields Figure 3.2 and is visually a more pleasing representation because pixels that do not have a significant projection onto either  $P_2$  or  $P_3$  appear desaturated or gray. This makes the image easier to view because naturally occurring scenes tend to be largely desaturated with low dimensionalities in the visible portion of the spectrum (Buchsbaum and Gottschalk, 1983).

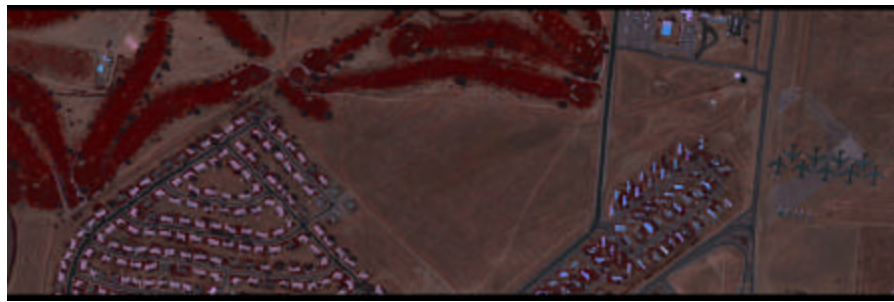


Figure 3.2. Pseudocolor Representation of Davis-Monthan Scene Obtained with Equation 3.1.

The mapping strategy in Figure 3.2 was designed with the performance of the human visual system in mind and does not present images that contain large regions of highly saturated hues that vary rapidly.

Utilizing the HYDICE bands of the original data corresponding approximately to the peak sensitivities of the  $\alpha$ ,  $\beta$ , and  $\gamma$  receptors, spectral bands 150, 38 and 10 respectively, we can display a scene that depicts approximately how we would perceive that scene if viewed directly. Figure 3.3 is a Red-Green-Blue image corresponding to bands 150, 38 and 10, which accurately portrays the landscape, as it would appear to the human observer.



Figure 3.3. RGB Image with Original Data Bands 150, 38 and 10.

Utilizing the RGB mapping strategy of Figure 3.3 and knowledge of linear transformations and eigenvectors from chapter two, we can identify a  $3 \times 3$  set of RGB eigenvectors for the individual scene. These statistics can then be applied to the RGB transformation of Equation 3.1 to produce an image that preserves the hue of the primary source of variance within the image (Figure 3.4). This mapping strategy retains the image display advantage achieved with Equation 3.1 and also allows for a straightforward method of mapping this scene into perceptual colorspace that preserves the expected hues for major scene constituents.



Figure 3.4. HSV Image Transformed with Scene RGB Data.

Keeping human visual perception and the characteristics of PCs in mind, it is clear that if a general set of PCs can be identified, a color mapping strategy can be arranged so that materials are presented in a straightforward manner, i.e. water can always be mapped to blue, vegetation to green, etc. As a wider range of wavelengths is considered, it should be expected that more than 3 PCs might be necessary to capture an equivalent amount of the data (99% or more). The next sections will investigate this and develop a coherent method for an invariant display methodology.

## B. ORIGINAL PRINCIPAL COMPONENTS STRATEGY

In the previous chapter the relationship between Hyperspectral Imaging and human color vision has been presented. Three statistically orthogonal channels can be produced by the PC analysis of the human photoreceptor spectral response. The first one is roughly achromatic representing luminosity, the second one being a difference between long- and mid-wavelength spectral content (red-green), and the third one being trimodal representing the difference between short- and mid-wavelength content (blue-yellow) (Buchsbaum and Gottschalk, 1983).

The above-mentioned orthogonal dimensions can be used to define the orthogonal directions in a 3-dimensional, conical data space. The three coordinates are hue, saturation, and value and give the location within the cone. The hue is defined as the angle with the R-G/B-Y plane, saturation is the radius in the R-G/B-Y plane divided by total intensity, and value represents the total intensity. These coordinates known as the H-S-V system can be used for constructing pseudocolor images.

The 1st PC usually related to the average scene illumination is derived by PC analysis of HSI data. Usually this channel has slow spectral variation and resembles closely the solar distribution convolved with the atmospheric response. An exception might appear to this general rule referring to the atmospheric absorption bands. However, when a particular material dominates an image, that spectral signature might also contribute significantly to the scene variance and may show up in the 1st PC as well.

At this point the present study attempts to introduce an improvement over the work done so far by utilizing an external eigenvector that could remove the atmospheric effects mentioned above. The points at which the original strategy needs to be improved and were not part of the previous study (Diersen, 2000) also include the reorientation of the hues wheel and the offset of the colorspace origin which as will be discussed later are vital for the invariability and accuracy of the pursued strategy.

### C. MODIFICATION USING EXTERNAL FIRST PC

The long-term goal of this project is the development of an invariant display strategy that can be generically applied to HSI data. The direct implementation of the method described in the previous section does not constitute an invariant strategy, since the Principal Components are calculated from *in scene* statistics. This results to a “biased” interpretation of the scene components that does not guarantee that materials are going to be presented in hues perceptive to the observer.

As a step in developing an invariant strategy, a standard 1<sup>st</sup> eigenvector that is computed from known solar and atmospheric properties was forced into the data. This was accomplished by means of a Gramm-Schmid orthogonalization whereby the covariance matrix of

$$\underline{\mathbf{y}} = \underline{\mathbf{x}} - \left( \underline{\mathbf{x}} \cdot \hat{\underline{\mathbf{v}}} \right) \hat{\underline{\mathbf{v}}} \quad (3.2)$$

was orthogonalized. In Equation 3.2  $\underline{\mathbf{x}}$  is the data vector and  $\hat{\underline{\mathbf{v}}}$  is a unit vector corresponding to the reference spectrum.

## 1. Scene Selection

In order to implement the invariant display strategy that is pursued by this study, a HYDICE Lake Tahoe image was selected. It consists of 320 lines of 320 pixels each and spreads over 210 bands through the visible and infrared spectrum. A view of the scene as it would appear to the human eye is shown in Figure 3.5 and it involves bands 46, 30 and 11.



Figure 3.5. Lake Tahoe Scene.

A certain part of the particular scene contains mainly pixels depicting water of the lake itself, while most of the rest of the scene contains pixels depicting vegetation. These two main parts are divided by narrow strips of bright sand and urban area. It is important to indicate that the water and vegetation parts of the scene are not homogeneous. Water

of varying depths can be seen gradually mixing with sand at shallower areas, while vegetation appears in various hues due to lighting conditions.

The particular Lake Tahoe scene is based only on raw data, which means that solar radiance and atmospheric absorption are included in the scene spectrum. Additionally, the scene contains significant light absorption in the infrared portion of the spectrum since it contains a significant amount of water pixels, while the widely abundant vegetation contributes with considerable absorption due to the presence of chlorophyll.

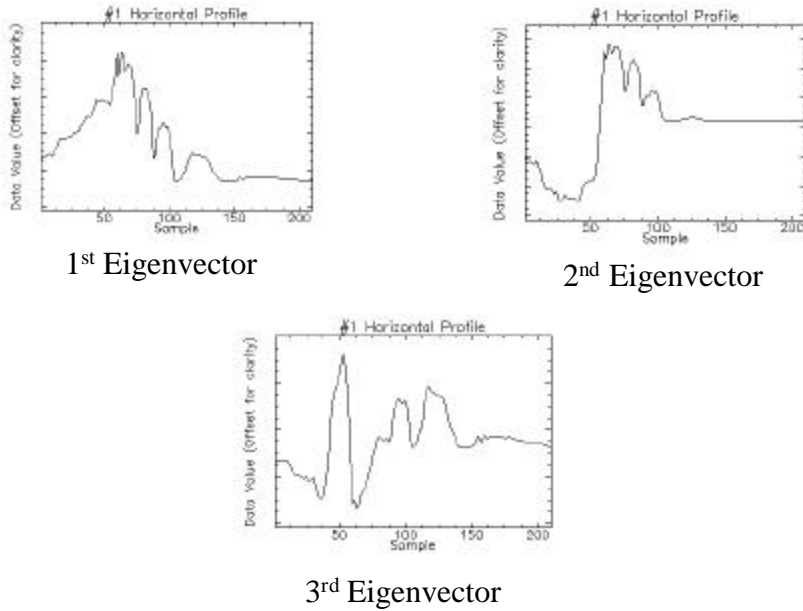


Figure 3.6. 1st, 2nd, and 3rd Eigenvectors from Tahoe Scene.

Implementing the PCA technique on the raw data of the above-mentioned Tahoe scene, using ENVI, the first three eigenvectors can be generated as shown in Figure 3.6. From the 1<sup>st</sup> eigenvector, which as aforementioned represents mainly the radiance of the scene, it becomes apparent that significant portions of radiance are missing due to the absorbent nature of the depicted elements. The above can be easier perceived after comparing the 1<sup>st</sup> eigenvector of the Tahoe scene to the respective eigenvector from the Davis-Monthan scene, as shown in Figure 3.7. The original Davis-Monthan scene, which

can be seen in Figure 3.8, as would appear to the human eye (bands 46, 30, and 11), contains mainly desert sand pixels and it can be hypothesized that the 1<sup>st</sup> eigenvector of this scene contains the solar radiance intact.

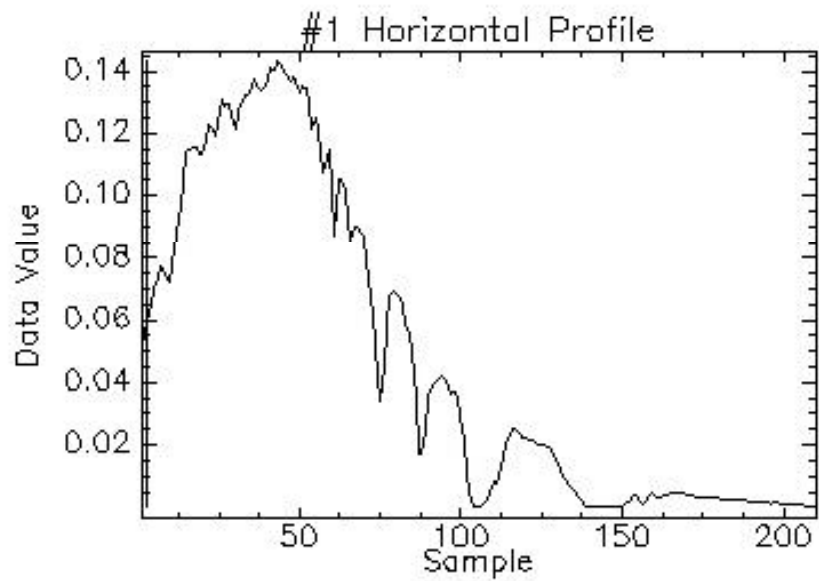


Figure 3.7. 1st Eigenvector from Davis-Monthan AFB Scene.

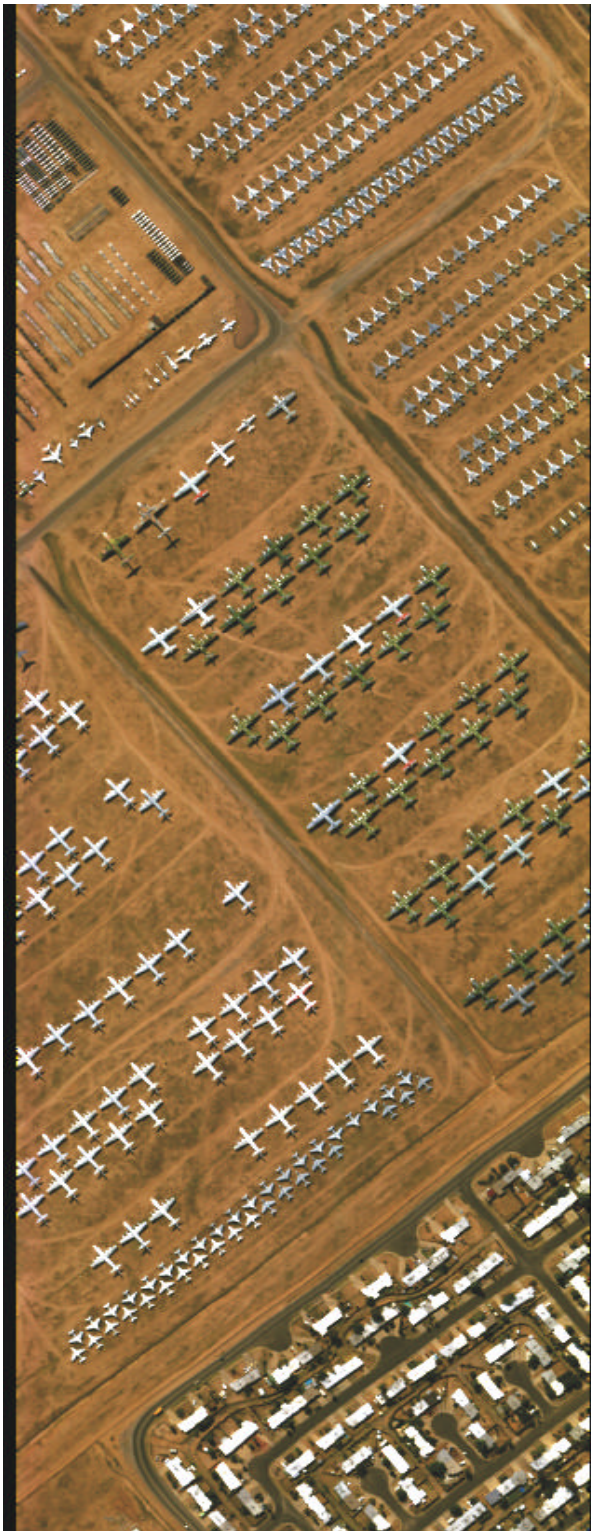


Figure 3.8. Davis-Monthan AFB Scene.

## 2. External Eigenvector Selection

As mentioned above, the scenes from the Davis-Monthan base area involve mainly desert sand pixels and therefore these scenes can be perceived as exhibiting negligible atmospheric and surface radiance absorption. Thus, a scene of this area can be utilized as the reference for solar radiance upon which all other scenes will be transformed in order to remove the absorption effects from them. The particular Davis-Monthan scene selected has already been shown in Figure 3.8 and its first three PC's are shown in Figure 3.9. It is interesting to note the similarities and differences of the respective sets of eigenvectors from the Tahoe scene and the Davis-Monthan scene. Comparing Figure 3.6 to Figure 3.9 it becomes apparent that the most important differences are concentrated in the 1<sup>st</sup> eigenvector, while the 2<sup>nd</sup> and 3<sup>rd</sup> eigenvectors exhibit minor differences mainly due to the dissimilar content of the two images.

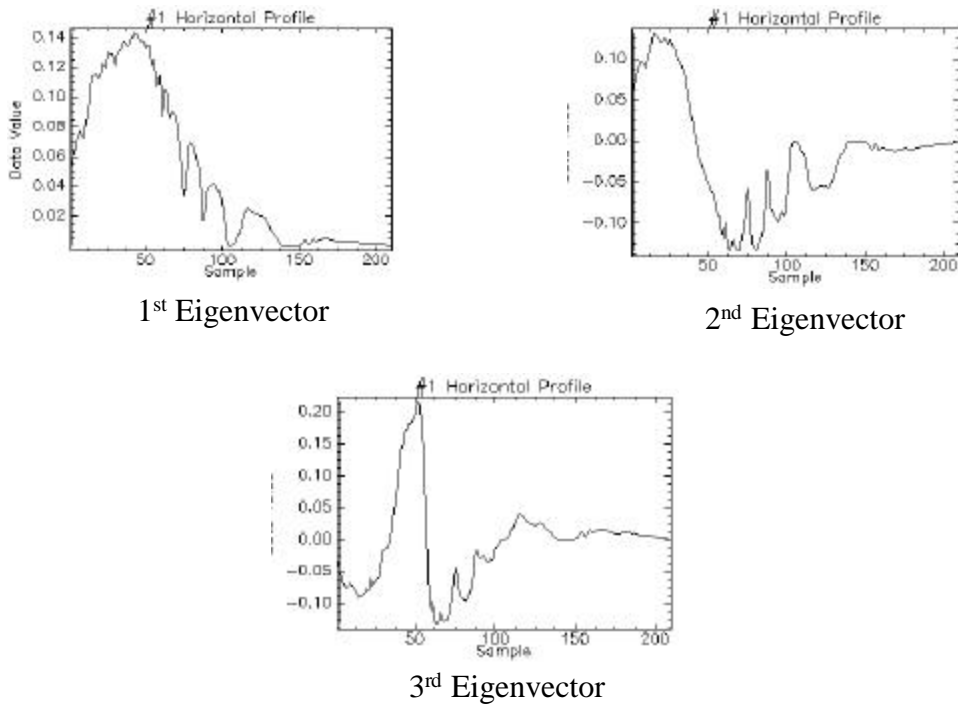


Figure 3.9. 1st, 2nd, and 3rd Eigenvectors from Davis-Monthan AFB Scene.

The broadband nature of the Davis-Monthan scene dictates its selection for the generation of the external eigenvector used in this study. In the long run the use of the output from a physics-based code, such as MODTRAN, would be preferred. That can provide an estimate of the mean solar radiance and atmospheric absorption spectra. Given

the environmental parameters at the time of collection, such as latitude, longitude day of the year time of the day, altitude, humidity, temperature, and look angle, MODTRAN can produce a spectrum based on the known solar spectrum and the predicted atmospheric composition and scattering. Such a spectrum would be optimally suited for generating an external eigenvector as described in this section.

### 3. Gramm-Schmidt Transform

The basis of this study is the removal of any *in scene* variable properties and the creation of a standard procedure that can lead to a true invariant display strategy. Therefore the 1<sup>st</sup> eigenvector from the Davis- Monthan scene presented above is going to be used as the standard vector bearing known solar and atmospheric properties, which is to be forced into the Lake Tahoe scene data. This is accomplished by means of Gramm-Schmidt orthogonalization as follows:

$$\underline{\mathbf{y}} = \underline{\mathbf{x}} - \left( \underline{\mathbf{x}} \cdot \hat{\underline{\mathbf{v}}} \right) \hat{\underline{\mathbf{v}}} \quad (3.2)$$

In Equation 3.2  $\underline{\mathbf{x}}$  represents the original Tahoe scene “cube” consisting of  $320 \times 320 \times 210$  elements reshaped to a  $102400 \times 210$  matrix form, while  $\hat{\underline{\mathbf{v}}}$  represents the 210-element-long 1<sup>st</sup> eigenvector from the Davis-Monthan scene. The resulting  $\underline{\mathbf{y}}$  is also a  $102400 \times 210$  matrix and in a similar fashion as  $\underline{\mathbf{x}}$  above, it can be reshaped into a  $320 \times 320 \times 210$ -element “cube”.

Utilizing ENVI it is possible to extract the eigenvectors for the new “projected” data in the same way as performed for the original data. The resulting 1<sup>st</sup>, 2<sup>nd</sup>, 3<sup>rd</sup>, and 210<sup>th</sup> eigenvectors are shown in Figure 3.10. Apparently the first two eigenvectors from the image yielded after the implementation of the projection technique are very similar to the 2<sup>nd</sup> and 3<sup>rd</sup> eigenvectors of the original scene as can be seen comparing Figures 3.6 and 3.10. Simultaneously the resulting 210<sup>th</sup> eigenvector of the new “projected” scene bears more similarities to the 1<sup>st</sup> eigenvector from the Davis-Monthan scene as can be seen comparing Figures 3.9 and 3.10.

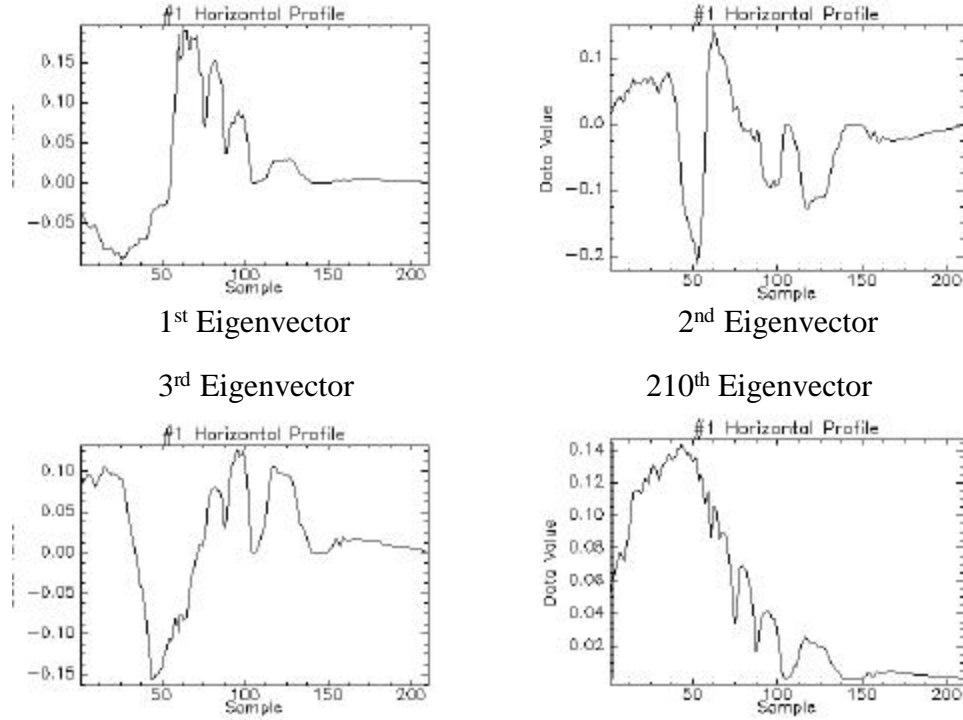


Figure 3.10. Resulting Eigenvectors from Gramm-Schmidt Transformation.

More important it can be proved that the new eigenvector is orthogonal to all the original scene eigenvectors except for the first one to which it is parallel. That means that the projection technique removed the solar radiance and atmospheric absorption elements from the 1<sup>st</sup> eigenvector—which was “pushed” to the bottom of the “stack” and those unwanted elements were redistributed evenly to the rest eigenvectors that have significantly less variance anyway.

#### 4. Scatter Plots

The resulting 1<sup>st</sup>, 2<sup>nd</sup>, and 210<sup>th</sup> are orthogonal to each other and thus can define a 3-dimensional space that can be depicted in the form of a scatter-plot. Using ENVI each pair of the three vectors can be combined to generate 2-dimensional scatter-plots as shown in Figure 3.11. From these three views the conical shape of the data cloud can become obvious.

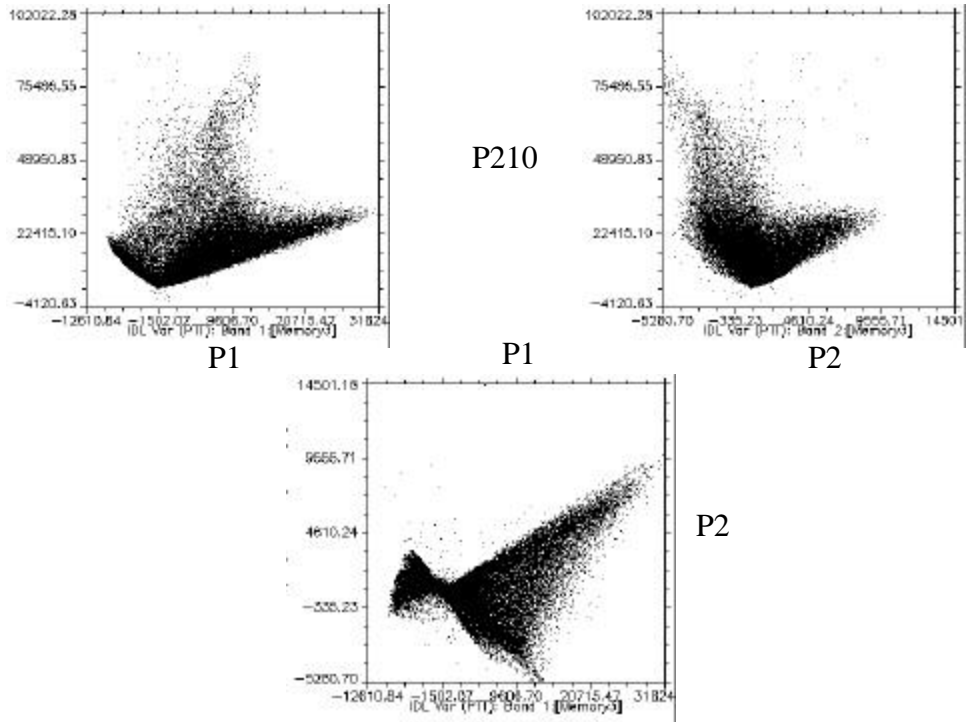


Figure 3.11. Scatterplots of the Resulting Eigenvectors.

These scatter-plots actually “pin-point” in the 3-dimensional space the exact value of the radiance contained in every pixel revealing the true nature of the material class depicted. It is interesting to mention that in this scene there are no pixels with zero radiance. At the same time there are clear lines radiating outward from the vertex of the cone indicating common classes of varying intensities (Tyo, et al., 2001).

Figure 3.11 contains three scatter plots generated by the eigenvector pairs P1-P210, P2-P210, and P1-P2, respectively. It is obvious that the bottom plot depicts the cone-shaped colorspace, or data cloud as seen from the cone’s vertex while the other two depict the colorspace from two lateral sides.

##### **5. n-Dimensional Visualizer and Endmembers Selection**

A generalization of the concept of the 2-dimensional scatter plot is provided by ENVI in the form of an interactive tool called n-Dimensional Visualizer™. As the various spectra can be thought of as points in an n-dimensional scatterplot, where **n** is the number of bands, the coordinates of the points in n-space consist of “n” values that are the spectral radiance in each band for a given pixel. The distribution of these points in n-space therefore can be used to estimate the number of spectral endmembers and their pure

spectral signatures. The n-Dimensional Visualizer allows for interactive rotation of data in n-dimensional space, selection of groups of pixels in classes, and collapsing of classes to make additional class selections easier. The selected classes can be exported to Regions of Interest (ROIs) and used as input into classification, unmixing or matched filtering techniques (Research Systems, ENVI Version 3.2 Manual, 1999).

With this tool it is possible to utilize up to all 210 bands available after the implementation of PCA. In this study the above-mentioned interactive tool was utilized using only the first two and the last (210<sup>th</sup>) eigenvectors, yielding the same scatterplots as in the 2-dimensional case described earlier. However in this case it became possible to deliberately and continuously rotate the resulting scatterplot in three dimensions revealing the structure of the colorspace in detail and thus clarifying which point formations corresponded to pure endmembers. Furthermore, the tool not only allowed for better isolation of pure endmembers but also their highlighting in distinct colors and their projection onto ROIs on the original scene. Figure 3.12 depicts the 3-dimensional scatter plot generated by the Visualizer and the highlighted endmembers corresponding to deep water (red), shallow water (yellow), dark vegetation (green), light vegetation (blue), and bright sand (thistle). The resulting ROIs on the Lake Tahoe image used for this scatterplot are shown in Figure 3.13 where the same colors are used to highlight the corresponding endmembers while the underlying image is shown in natural color as perceived by the human vision.

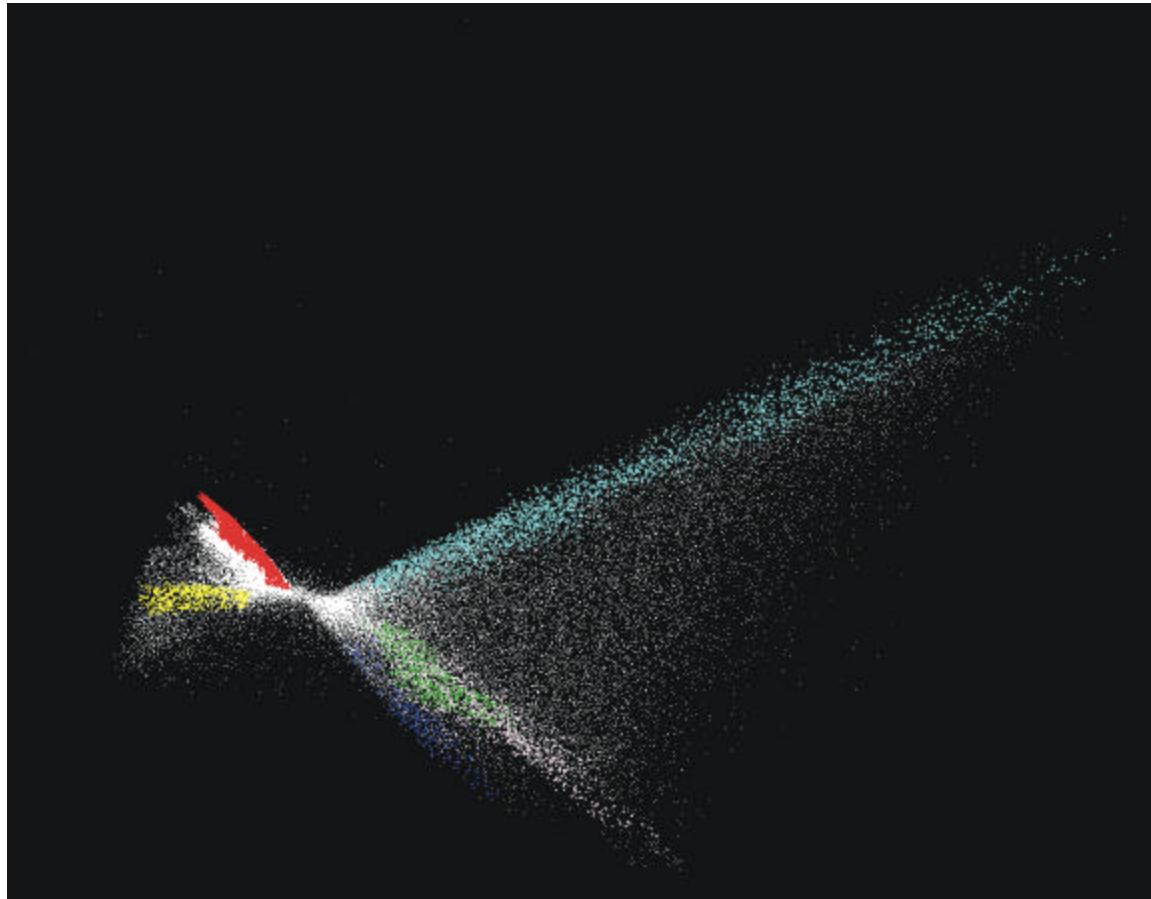


Figure 3.12. Endmembers as Highlighted by n-D Visualizer.

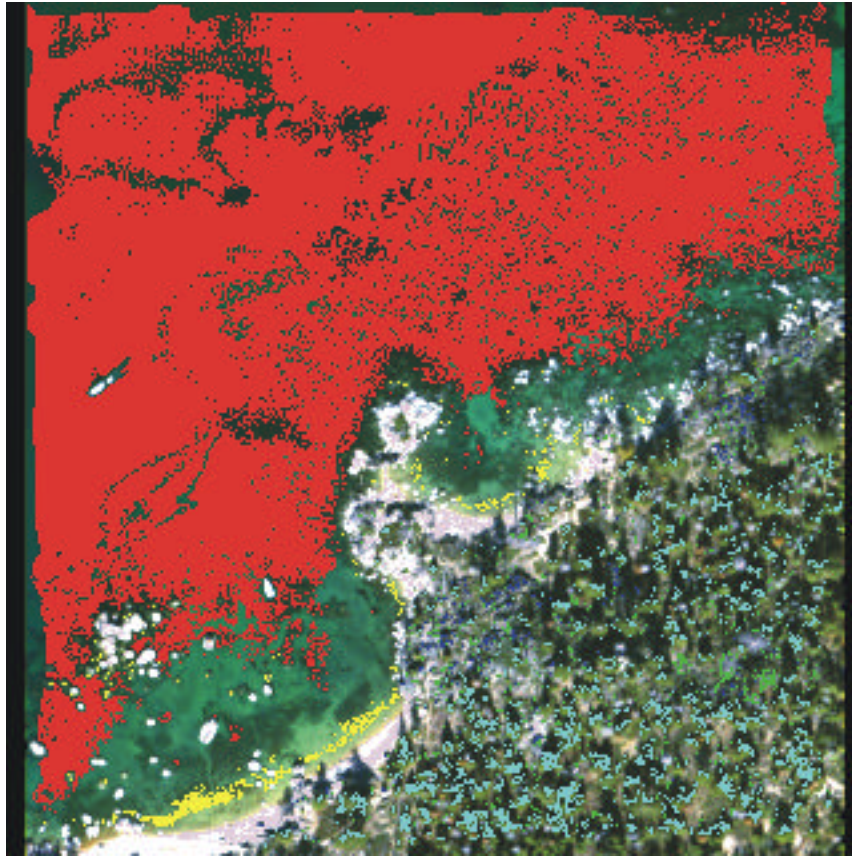


Figure 3.13. ROIs Highlighted by the n-D Visualizer.

## 6. Cone Vertex Coordinates Determination

As can be seen in Figures 3.11 and 3.12 the scatterplots demonstrate classes of data radiating out from a common point along particular directions relative to the longitudinal (P210 vector) axis. Furthermore, as the overall intensity (value of P210) increases, the distance from the P210 axis increases, but the angle with respect to that axis remains the same. This type of geometrical symmetry is suggestive of a cone.

Upon further investigation of the PC transformation, such a conical nature of the data should be expected. The first eigenvector is guaranteed to be all positive, and as discussed previously is usually closely related to the mean atmospheric spectrum. When dealing with spectral imagery data, this eigenvector usually contains 90% or more of the scene variance. The successively higher eigenvectors represent axes that are transverse to the first. They correspond to significantly smaller eigenvalues, so the displacement along these axes is generally much smaller than the displacement in the P210 direction. Since

the P1 and P2 eigenvectors represent deviations from the approximate mean spectrum, the relative values of the projection of a particular material in these directions should be approximately constant as the intensity increases, i.e.

$$\frac{\mathbf{P2}}{\mathbf{P1}} \cong \text{cons tant} \quad (3.3)$$

as the intensity increases. Furthermore, the linear nature of the PC transform suggests that

$$\frac{\sqrt{\mathbf{P1}^2 + \mathbf{P2}^2}}{\mathbf{P210}} \cong \text{cons tant} \quad (3.4)$$

as the intensity increases. It is clear that these relations are being mapped into the Hue and Saturation, respectively (as in Equation 3.1), so the mapping proposed in Equation 3.1 is well suited to a dataspace that is conical. This should not be surprising, as the Hue, Saturation, and Value coordinate system is essentially a descriptor of the cone of allowable colors.

Using the scatterplots method yields a very good perception of the colorspace defined by the data cloud and as previously mentioned the endmembers can be readily distinguished. However, conical-shaped data cloud is not always centered at the origin of the dataspace being used. As a matter of fact producing an “off-center” data cloud is rather common. The above results into the inability to correctly assign the color directions to the cloud patterns that correspond to the various endmembers. For example, if it is attempted to assign color directions to the data cloud shown in Figure 3.12 where the dataspace origin is different than the vertex of the data cloud cone, the resulting direction lines will cross more than one of the highlighted endmember patterns resulting in false assumptions about the hue representation of these endmembers.

A method was devised and used in this study to determine, as accurately as possible, the coordinates of the conical colorspace vertex and from that define the directions needed to assign hue representations to the endmembers correctly. This method is rather semi-autonomous since it is needed to manually identify pixels with like spectral characteristics corresponding to the same endmember. The data cloud shown above in Figure 3.12 is now shown in Figure 3.14 in a “trimmed-down” fashion where the various

endmembers previously mentioned have been highlighted in the same colors while the cloud is viewed from a slightly different angle.

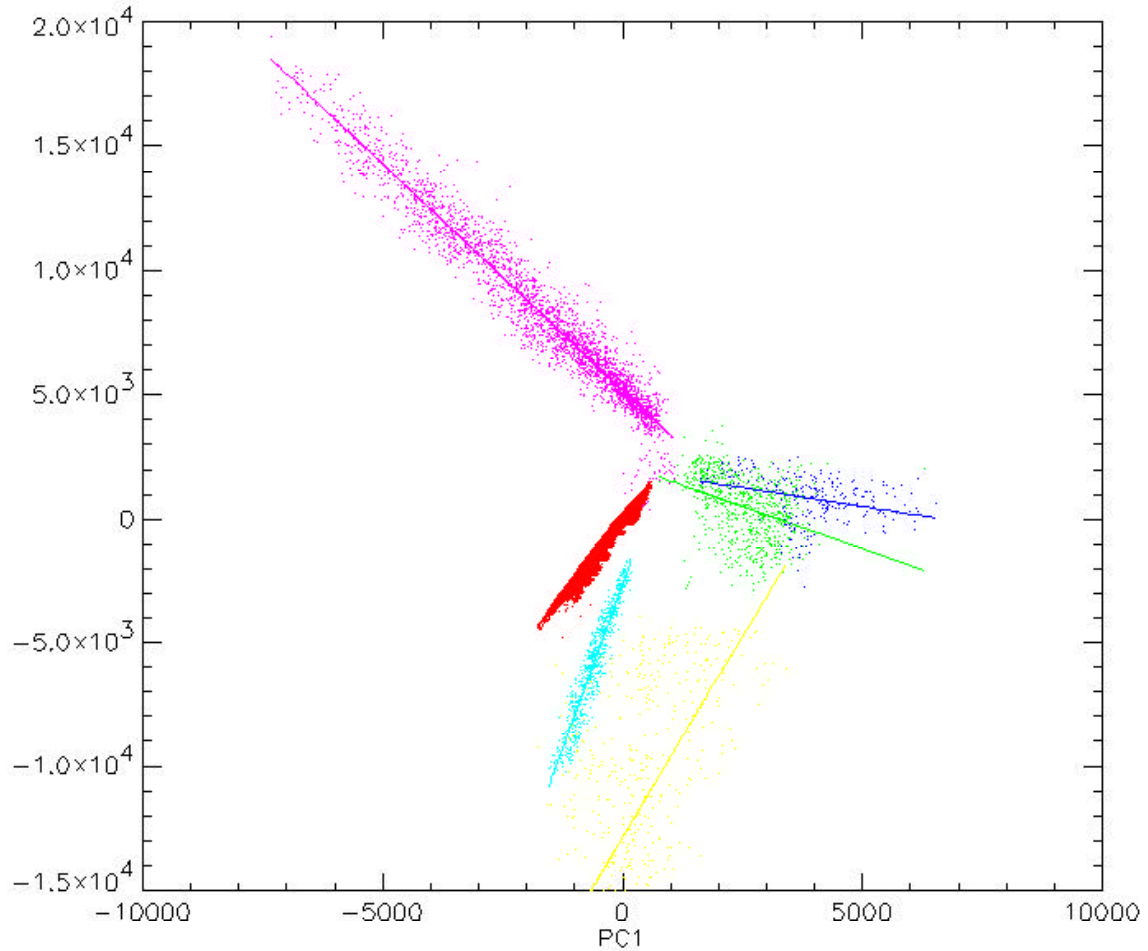


Figure 3.14. Trimmed-down Data Cloud Indicating MSE Approximations.

Three of these pixel groups, namely deep water (red), light vegetation (blue), and bright sand (thistle) that apparently lie in much separated directions can be utilized for the vertex determination approach. For each of the above-mentioned pixel groups, the least-square regressions were computed automatically using IDL programming. The same routine was executed for all three projections resulting in a 3-dimensional approach. Figure 3.15 shows the resulting directions from the regressions in the three orthogonal planes.

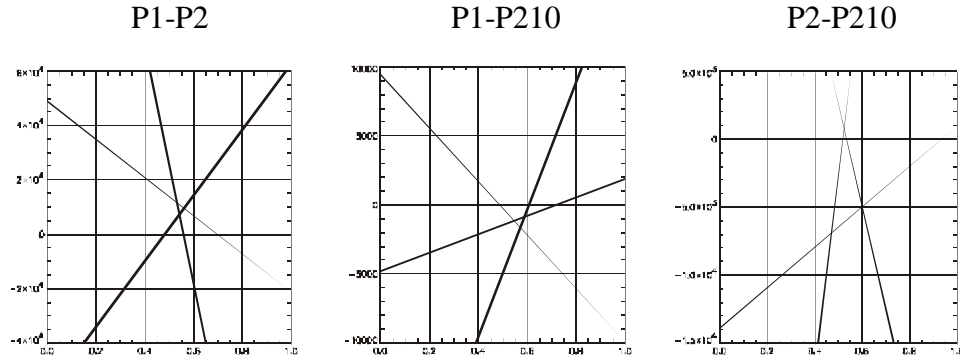


Figure 3.15. Selected Directions Approximating Cone Vertex in 3-Dimensions.

In a rather subjective manner and from these plots, the vertex of the cone was estimated to lie at the coordinates

$$(x, y, z)=(2000, 5000, 6000) \quad (3.5)$$

relative to the dataspace origin.

## 7. Data Shifting

Implementing the above technique resulted in the approximate determination of the colorspace cone vertex and thus the only step needed to be taken in order to “normalize” the data, is to literally shift the whole data cloud to the dataspace origin. This can be achieved either by shifting the original scene data altogether or by shifting only the resulting projected eigenvectors for as much as calculated above. The first method would be rather tedious therefore the shifting in three dimensions of the only three eigenvectors of interest-P1, P2, and P210-was executed. Since P1 and P2 define the “base” of the conical cloud, they were shifted by  $x=y=5000$  units each, while P210 which represents the longitudinal axis of the cone was shifted by  $z=6000$  units. Therefore, the new set of eigenvectors relates to the older one as follows:

$$P_{1\text{new}}=P_1-2000, \quad P_{2\text{new}}=P_2-5000, \quad P_{210\text{new}}=P_{210}-6000 \quad (3.6)$$

The overall shape of the conical colorspace has been preserved while its vertex lies as close to the origin of the dataspace as possible. Also the orientation of the cloud has been preserved since no rotation took place.

### 8. HSV System Determination

The previously presented technique eventually yields an orthogonal set of three eigenvectors that define accurately the colorspace of the scene under study after the removal of radiance and atmospheric absorption from the original image and the consequent shift of the data relative to the origin of the dataspace. Utilizing this eigenvector set and Equation 3.1 a new HSV(Hue-Saturation-Value) system is produced that enables the invariant display of the Lake Tahoe scene. The system forms as follows:

$$\begin{aligned} \theta = \mathbf{a} \tan \left( \frac{\mathbf{P}_{2\text{new}}}{\mathbf{P}_{1\text{new}}} \right) &\rightarrow H_{\text{new}} \\ \frac{\sqrt{\mathbf{P}_{1\text{new}}^2 + \mathbf{P}_{2\text{new}}^2}}{\mathbf{P}_{210\text{new}}} &\rightarrow S_{\text{new}} \\ \mathbf{P}_{210\text{new}} &\rightarrow V_{\text{new}} \end{aligned} \quad (3.7)$$

At this point the resulting system would be adequate for human eye visualization since it corresponds to the way images are naturally perceived, as developed earlier in the corresponding section. However in an artificial environment like IDL and ENVI the HSV system cannot be utilized directly to produce an image. Therefore a transformation needs to be performed from the HSV into an ENVI-perceivable RGB system.

### 9. HSV to RGB Transformation

In order to make possible for the processed image to be effectively displayed by the ENVI software, a pixel-by-pixel transformation was implemented utilizing the previously presented HSV data in a normalized fashion. Therefore the data to be transformed consisted of the H, S, and V values of each pixel on domain [0, 1], while the output of the transformation consisted of the R, G, and B values on range [0, 1]. The transformation was implemented through the programming concept outlined in Table 3.1 (Smith, A. R., 1978). In order to be consistent with rest of the execution of this study, the

transformation described in this section was implemented with IDL programming. MATLAB programming can be utilized for this purpose as well.

**H:=6\*H**

**I:=floor(H)**

**F:=H-I**

**M:=V\*(1-S)**

**N:=V\*(1-(S\*))**

**K:=V\*(1-(S\*(1-F)))**

**Case 0: (R,G,B):=(V,K,M)**

**Case 1: (R,G,B):=(N,V,M)**

**Case 2: (R,G,B):=(M,V,K)**

**Case 3: (R,G,B):=(M,N,V)**

**Case 4: (R,G,B):=(K,M,V)**

**Case 5: (R,G,B):=(V,M,N)**

Table 3.1. HSV to RGB Transformation.

## 10. RGB Visualization

The produced sets of (R,G,B) values using the above described transformation can be readily introduced into ENVI software as three distinctive grayscale images (R-image, G-image, and B-image) consisting of 320×320 pixels each. The images can be seen in Figure 3.16, each highlighting slightly different aspects of the same scene. ENVI can combine these three images and yield the final color image shown in Figure 3.17. In fact, in order to obtain an image like this a minor “intervention” by the operator was needed adjusting the hue wheel orientation so that a human observer would easily perceive the resulting colors.



Figure 3.16. R, G, B Images.



Figure 3.17. Processed and Rotated Color Image.

Although the image produced by the software had correctly assigned colors onto the various classified materials depicted, these colors did not correspond to the hues commonly associated to the particular materials. For example the body of the lake water was depicted as red although the particular color was correctly assigned to the entire body of water. Therefore, a shift of the hues was needed, in a rather humanly subjective manner, so that water would be presented in blue, for example, while the hue shift was performed in a constant angle throughout the hue wheel. A way of achieving such a hue shifting without the intervention of the operator could be the subject of future work.

THIS PAGE INTENTIONALLY LEFT BLANK

#### **IV. LIMITATIONS AND FUTURE WORK**

The technique developed and outlined by this study represents one further step towards the long-term goal of the parent project, which is the development of an invariant display strategy capable of being broadly applied to hyperspectral data of any kind.

The present study continued from the point that previous studies had reached and the principal contribution compared to them is the research into the utilization of *in-scene* vs. *non-in-scene* eigenvectors. It has already been concluded that the derived eigenvectors are different for every selected scene even though among various scenes a great amount of spectral correlation might exist and therefore similar spectra would exhibit different representations from one image to another. Furthermore, comparison between dissimilar scenes yields severe differences. Ultimately the development of a set of orthogonal eigenvectors capable of capturing the most part of the spectral information in various scenes could be achieved and applied to a variety of research. A standard mapping could be developed, therefore, using these eigenvectors resembling the “tasseled cap” transformation frequently applied to multispectral imagery, namely LANDSAT data (Kauth and Thomas, 1976). However such a goal presents a great amount of effort and it does not seem to be a matter of the very near future mainly due to the enormous size of data to be processed and the higher dimensionality of hyperspectral vs. multispectral imagery.

This study made clear that the introduction of eigenvectors not related to the scene under processing improved the invariability of the final display by removing features inherent to the target spectra deviating significantly from the mean solar spectrum, thereby biasing and smearing the overall color representation. A careful selection of the scene from which the external eigenvector is selected might be an important factor influencing the final outcome of the display strategy. The above statement was clearly demonstrated by selecting the Davis-Monthan scene external eigenvector, which exhibited fairly smooth and relatively homogeneous spectral characteristics. The Lake Tahoe scene that was processed in this study exhibited a

significant deviation from the mean spectrum, mainly because of the water absorption in the infrared region and because of the characteristic chlorophyll absorption line.

The Gramm-Schmidt transformation that was implemented allowed the external eigenvector from the Davis-Monthan scene to force this scene-specific information into the second and third eigenvectors of the Tahoe scene and thus yield a new first eigenvector that exhibited very small, if any, deviation from the mean solar spectrum. Since the most part of the radiance contained in an image concentrates in its first eigenvector, the above-mentioned technique resulted in a practically unbiased representation emphasizing more on the various endmember spectra differences. Eventually this leads closer to the invariability sought by the parent project.

The features available in the ENVI software package provided a significant amount of assistance towards the approach followed in this study. Use of the readily available scatterplots among the three principle eigenvectors generated as well as the n-dimensional visualizer tool allowed quick and accurate determination of the constituent spectra within an image and their respective hue directions in the colorspace cone. These techniques simplified the task of the colorspace origin estimation relative to the general dataspace leading to a reconstruction of the original image color representation on a more invariant fashion.

Figure 4.1 presents the overall outcome of the technique devised and followed comparing the original Lake Tahoe scene as would be perceived by the human vision (top) to the processed image (bottom). Apparently the various deviations of the water part of the image have been removed as well as most of the ambiguities in the shore part between vegetation shoreline and urban spots. In this case a human analyst would be able to perceive the real content of the scene without any further processing since the major constituents of the image are clearly distinguished from each other and color marked according to common sense. Therefore the lake water is depicted as blue in its entirety, the forest and the rest of the vegetation as green, and so forth.

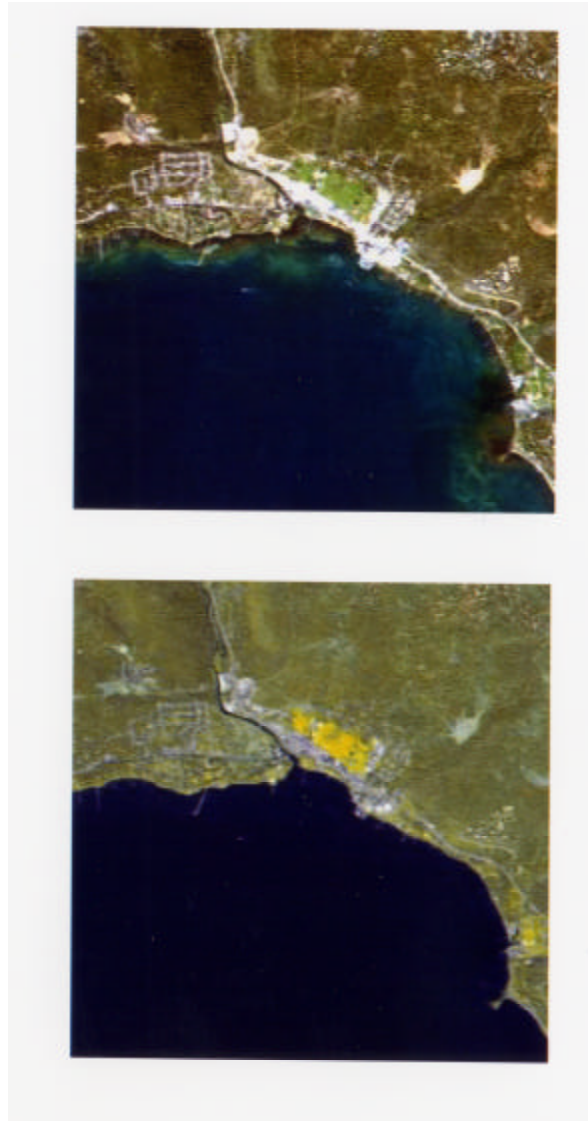


Figure 4.1. Images Comparison: Top-Original Image, Bottom-Processed Image.

However these results do not constitute the ultimate solution to the problem of the invariant strategy since some important steps had to be taken outside the “automated flow” of action. Originally the selection of the Davis-Monthan external eigenvector was arbitrary and based on totally subjective criteria. Ideally, a thorough study should have preceded the selection of the external eigenvector yielding one optimally resembling clear solar spectrum. It has already been mentioned that a promising approach would be utilizing physics-based software such as MODTRAN which determines mean solar radiance and atmospheric absorption figures based on the exploitation of environmental

parameters on the particular time of the particular scene exposure. Such an application would be the focus of future work on the topic.

Additionally significant “manual” intervention occurred during the determination of the conical colorspace vertex and the subsequent hue wheel turn. As described in the previous section, the operator had to select the number and the kind of the endmember spectra whose approximation and projection determined the colorspace origin. Even minor ambiguities in this process might result in hue smearing affecting the judgment about the hue wheel turn as well. In the example described here the minimum number of endmember spectra was selected (namely, three) and their hues were as different as possible so that they would yield a fairly accurate result. However, in order to generalize the process for various scenes, a more thorough selection with a greater number of more accurately defined endmember spectra should be made. The ultimate external intervention in the whole display process was the hue wheel turn so that the naturally occurring colors would be matched. This adjustment is completely subjective to the human operator’s perception and could not be duplicated in a software-controlled fashion.

## V. SUMMARY AND CONCLUSIONS

The principal components-based mapping strategy discussed in this study constitutes a relatively simple technique to perform unsupervised classification for a wide variety of hyperspectral imagery. In this way the analyst can perceive the true content of a scene and direct attention to particular areas for further processing and analysis. The introduction of an external eigenvector into the analysis procedure results in further invariance of the process, removing the need for an interim analysis of the data dependent on the *in-scene* statistics. Furthermore the supervised shifting of the resulting data and the hue adjustments in the final image provided with a practical way of achieving an invariance of the display strategy indicating at the same time the directions on which the follow-on studies should move.

As discussed in the previous sections there are still several topics to be addressed and resolved before a fully unsupervised and invariant display technique is operationally functional. Research ought to be conducted on the performance of the latest technique on a variety of scenes with diverse spectral content. Although the function of covariance was implemented in this study to generate the necessary statistics, it would be interesting to investigate the performance of a technique utilizing correlation or even based on the logarithm of the original data cubes.

Another issue that needs to be refined is the selection of the external eigenvector, which should imitate the solar spectral characteristics as closely as possible and a reasonable approach to that would be the combination of data from various scenes into a synthetically generated eigenvector.

Finally the goal of creating a truly unsupervised methodology would be attained among others by devising software-based ways of accurately pinpointing the origin of the colorspace by utilizing a fairly large number of carefully defined spectral endmembers. Ultimately the research trend followed should also tackle the demanding task of the rotation of the final image hues in a way that human perception would readily assume knowledge of the scene under analysis. At this point, although the current technique manages to yield images that are spectrally color-defined and distinguished, the analyst

definitely needs to predetermine the connection of the various hues to the materials represented.

## LIST OF REFERENCES

- Anderson, T. W., *An Introduction to Multivariate Statistical Analysis*, Second Edition, John Wiley & Sons, New York, NY, 1984.
- Brainard, D. H., Wandell, B. A., and Chichilnisky, "Color Constancy: From Physics to Appearance," *Current Directions in Psychological Science*, pp. 165-170, October 1992.
- Brower, B V., Haddock, D. H., Reitz, J. P., and Schott, J., "Spectrally and Spatially Adaptive Hyperspectral Data Compression," *SPIE Proceedings*, vol. 2821, August, 1996.
- Buschbaum, G., and Gottschalk, A., "Trichromacy, Opponent Colours Coding and Optimum Colour Information Transmission In The Retina" *Proc. R. Soc. Lond. B* 220, pp. 89-113, 1983.
- Diersen, D. I., *An Invariant Display Strategy for Hyperspectral Imagery*, Master's Thesis, Naval Postgraduate School, Monterey, California, December 2000.
- Fukunaga, K., *Introduction to Statistical Pattern Recognition*, Academic Press, New York, NY, 1972.
- Goetz, A. F. H., "Imaging Spectrometry for Remote Sensing: Vision to Reality in 15 Years." *Proceedings of SPIE*, vol. 2480: *Imaging Spectrometry*, pp. 2-13, 1995.
- Golub, G. H., and Van Loan, C. F., *Matrix Computations*, Johns Hopkins University Press, Baltimore, MD, 1983.
- Gorman, J. D., Subotic, N. S., and Thelen, B. J., "Robust Material Identification in Hyperspectral Data via Multiresolution Wavelet Analysis," 1995 *International Conference on Acoustics, Speech, and Signal Processing Proceedings*, vol. 5, pp. 2805-2808, May 9-12, 1995.
- Haykin, S., *Adaptive Filter Theory*, Third Edition, Prentice Hall, Upper Saddle River, NJ, 1996.
- Hotelling, H., "Analysis of Complex Statistical Variables into Principal Components," *The Journal of Educational Psychology*, vol. 24, pp. 417-441 and 498-520, September and October 1933.
- Jenson, S. K., and Waltz, F.A., "Principal Components Analysis and Canonical Analysis in Remote Sensing," *Proceedings of the American Society of Photo Grammetry, 45<sup>th</sup> Annual Meeting*, pp.337-348, 1979.
- Jolliffee, I. T., *Principal Component Analysis*, Springer-Verlag, New York, NY, 1986.
- Kauth, R. J., and Thomas, G. S., "The Tasseled Cap-A Graphical Description of the Spectral-Temporal Development of Agricultural Crops As Seen by Landsat," *Proceedings of the Symposium on Machine Processing of Remotely Sensed Data*, pp. 4B41-4B51, Purdue University, (West LaFayette, IN), 1976.
- Kapur, J. N., *Maximum-Entropy Models in Science and Engineering*, John Wiley & Sons, New York, NY, 1989.

- Krauskopf, J., Williams, D. R., and Heeley, D. W., "Cardinal Directions of Color Space," *Vision Res.* 22, pp. 1123-1131, 1982.
- Leon-Garcia, A., *Probability and Random Processes for Electrical Engineering*, Second Edition, Addison-Wesley, Reading, MA, 1994.
- Rao, A. K., and Bargava, S., "Multispectral Data Compression Using Bidirectional Interband Prediction," *IEEE Transactions on Geoscience and Remote Sensing*, vol. 34, no. 2, pp. 385-397, March 1996.
- Ready, P. J., and Wintz, P. A., "Information Extraction, SNR Improvement, and Data Compression in Multispectral Imagery," *IEEE Transactions on Communications*, vol. COM-21, no 10, pp. 1123-1130, October 1973.
- Research Systems, Inc., Boulder, CO., *Interactive Data Language User's Guide*, Version Four, March 1995.
- Research Systems, Inc., Boulder, CO, *ENVI Manual*, Version 3.2, July, 1999.
- Richards, J. A., *Remote Sensing Digital Image Analysis*, Springer-Verlag, New York, NY, 1993.
- Rinker, J. M., "Hyperspectral Imagery. What is it? What Can I Do?" *USA CE Seventh Remote Sensing Symposium*, May 7-9, 1990.
- Scharf, L. L. *Statistical Signal Processing: Detection, Estimation, and Time-Series Analysis*, Addison-Wesley, Reading, MA, 1991.
- Searle, S. R., *Matrix Algebra Useful for Statistics*, John Wiley & Sons, New York, NY, 1982.
- Singh, A., and Harrison, A., "Standardized Principal Components," *International Journal of Remote Sensing*, vol. 6, no. 6, pp. 883-896, 1985.
- Smith, A. R., "Color Gamut Transform Pairs," *Computer Graphics*, vol.12, no 3, pp. 12-19, August 1978.
- Smith, M. O., Johnson, P. B., and Adams, J. B., "Quantitative Determination of Mineral Types and Abundances from Reflectance Spectra Using Principal Components Analysis," *Proceedings of the 15<sup>th</sup> Lunar and Planetary Science Conference, Part 2, Journal of Geophysical Research*, vol.90 supplement, pp. C797-C804, February 1985.
- Stefanou, M. S., *A Signal Processing Perspective of Hyperspectral Imagery Analysis Techniques*, Master's Thesis, Naval Postgraduate School, Monterey, California, June 1997.
- Therrien, C. W., *Discrete Random Signals and Statistical Signal Processing*, Prentice Hall, New York, NY, 1992.
- Tyo, J. S., Pugh, E. N., Engheta, N, "Colorimetric Representation for Use with Polarization-Difference Imaging in Scattering Media," *J. Opt. Soc. Am. A*, vol. 15, pp. 367-374, 1998.
- Tyo, J. S., Diersen, D. I., Olsen, R. C., "Development of an Invariant Display Strategy for Spectral Imagery" *Proceedings of SPIE*, vol. 4132: *Imaging Spectrometry VI*, August 2000.

Tyo, J. S., Konsolakis, A. E., Diersen, D. I., Olsen, R. C., "Invariant Display Strategy for Spectral Imagery" *Proceedings of SPIE*, vol. 4480: *Imaging Spectrometry VII*, August 2001.

Vane, G., and Goetz, A. F. H., "Terrestrial Imaging Spectroscopy," *Remote Sensing of the Environment*, vol. 24, pp. 1-29, 1988.

Wald, G., "Human Vision and the Spectrum," *Science*, vol. 145, 3636, pp.1007-1017, September 1964.

Watkins, D. S., *Fundamentals of Matrix Computations*, John Wiley & Sons, New York, NY, 1991.

Wyszecki, G., and Stiles, W. S., *Color Science*, Wiley, New York, NY, 1967.

THIS PAGE INTENTIONALLY LEFT BLANK

## **INITIAL DISTRIBUTION LIST**

1. Defense Technical Information Center  
Ft. Belvoir, Virginia
2. Dudley Knox Library  
Naval Postgraduate School  
Monterey, California
3. Chairman, Code EC, Department of Electrical and Computer Engineering  
Naval Postgraduate School  
Monterey, California  
[jknorr@nps.navy.mil](mailto:jknorr@nps.navy.mil)
4. Dr. Roberto Cristi, Code EC, Department of Electrical and Computer Engineering  
Naval Postgraduate School  
Monterey, California  
[rchristi@nps.navy.mil](mailto:rchristi@nps.navy.mil)
5. Captain J. Scott Tyo, USAF, Department of Electrical and Computer Engineering  
Naval Postgraduate School  
Monterey, California  
[tyo@eece.unm.edu](mailto:tyo@eece.unm.edu)
6. R. C. Olsen, Code PH, Department of Physics  
Naval Postgraduate School  
Monterey, California  
[olsen@nps.navy.mil](mailto:olsen@nps.navy.mil)
7. Lieutenant Athanasios E. Konsolakis, Hellenic Navy  
Naval Postgraduate School  
Monterey, California  
[akonsola@nps.navy.mil](mailto:akonsola@nps.navy.mil)
8. Embassy of Greece  
2228 Massachusetts Avenue, N. W.  
Washington, DC, 20008  
[grnavat@aol.com](mailto:grnavat@aol.com)